



## OPEN A new intelligent control strategy for CSTH temperature regulation based on the starfish optimization algorithm

Davut Izci<sup>1,2,3</sup>, Serdar Ekinci<sup>4</sup>, Mostafa Jabari<sup>5</sup>, Mohit Bajaj<sup>6,7,8</sup>✉, Vojtech Blazek<sup>9</sup>, Lukas Prokop<sup>9</sup>, Ali Riza Yildiz<sup>10</sup> & Seyedali Mirjalili<sup>11,12</sup>

Temperature regulation in nonlinear and highly dynamic processes such as the continuous stirred-tank heater (CSTH) is a challenging task due to the inherent system nonlinearities and disturbances. This study proposes a novel metaheuristic-driven control strategy, combining the two degrees of freedom-PID acceleration (2DOF-PIDA) controller with the recently developed starfish optimization algorithm (SFOA) for temperature control of the CSTH process. The 2DOF-PIDA controller enhances system performance by decoupling setpoint tracking and disturbance rejection, while the SFOA ensures optimal tuning of controller parameters by leveraging its powerful exploration and exploitation capabilities. Simulation results validate the effectiveness of the proposed approach, demonstrating improved tracking accuracy, disturbance rejection, and robustness compared to conventional methods. The combination of 2DOF-PIDA and SFOA provides a flexible and efficient solution for controlling highly nonlinear systems, with significant implications for industrial temperature regulation applications.

**Keywords** Nonlinear continuous stirred-tank heater (CSTH), Starfish optimization algorithm (SFOA), Temperature control of highly nonlinear system, Two degrees of freedom-PID acceleration (2DOF-PIDA) controller

### List of symbols

$\rho$	Tank fluid density
$\rho_c$	Heating fluid density
$D$	Tank diameter
$A$	Tank inside section area
$A_c$	Jacket heat transfer area
$C_p$	Tank fluid heat capacity
$C_{pc}$	Heating fluid heat capacity
$g$	Gravity constant
$K_L$	Level transmitter gain
$K_T$	Temperature transmitter gain
$K_{vL}$	Level control valve constant
$K_{vT}$	Temperature control valve constant
$K_{xL}$	Level control valve stem constant
$K_{xT}$	Temperature control valve stem constant

<sup>1</sup>Department of Electrical and Electronics Engineering, Bursa Uludag University, Bursa 16059, Turkey. <sup>2</sup>Applied Science Research Center, Applied Science Private University, Amman 11931, Jordan. <sup>3</sup>Jadara University Research Center, Jadara University, Irbid, Jordan. <sup>4</sup>Department of Computer Engineering, Batman University, Batman 72100, Turkey. <sup>5</sup>Faculty of Electrical Engineering, Sahand University of Technology, Tabriz, Iran. <sup>6</sup>Department of Electrical Engineering, Graphic Era (Deemed to be University), Dehradun 248002, India. <sup>7</sup>College of Engineering, University of Business and Technology, Jeddah 21448, Saudi Arabia. <sup>8</sup>Graphic Era Hill University, Dehradun 248002, India. <sup>9</sup>ENET Centre, CEET, VSB-Technical University of Ostrava, Ostrava 708 00, Czech Republic. <sup>10</sup>Department of Mechanical Engineering, Bursa Uludag University, Bursa 16059, Turkey. <sup>11</sup>Centre for Artificial Intelligence Research and Optimisation, Torrens University Australia, Brisbane, Australia. <sup>12</sup>University Research and Innovation Center, Obuda University, Budapest 1034, Hungary. ✉email: mohitbajaj.ee@geu.ac.in

$Q_i$	Normal tank inlet fluid flow rate
$T_i$	Fluid inlet temperature
$T_{ci}$	Heating fluid inlet temperature
$T_{sp}$	Temperature controller set-point
$T_L$	Level transmitter time constant
$T_T$	Temperature transmitter time constant
$T_{vL}$	Level control valve time constant
$T_{vT}$	Temperature control valve time constant
$P_{cp}$	Heating fluid pump discharge pressure
$P_{cr}$	Heating fluid system return pressure
$R_c$	Heating system pipe nominal flow resistance
$R_{vT}$	Temperature control valve rangeability
$U$	Overall heat-transfer coefficient
$V_c$	Heat jacket volume
$W_c$	Heating jacket wide
$H_c$	Heating jacket height
$H_t$	Tank wall height
$H_{sp}$	Level controller set-point
$M$	Fluid mass in the tank
$\beta$	Weighting factor for proportional term sensitivity to setpoint changes
CF	Cost function
$O_{s,norm}$	Normalized percent overshoot
$E_{ss,norm}$	Normalized percent steady-state error
$t_{set,norm}$	Normalized settling time
$t_{rise,norm}$	Normalized rise time
$N_{ps}$	Population Size
$T_{max}$	Maximum Iteration
MSA	Mantis Search Algorithm
$u(t)$	Control signal (heating power)
$K_p$	Proportional gain
$\beta$	Weighting factor for setpoint tracking
$T$	Measured temperature of the fluid
$dT$	Rate of change of the measured temperature
$dT_{set}$	Rate of change of the setpoint temperature
$Q_{in}$	Inlet flow rate
$Q_{out}$	Outlet flow rate
$T_t$	Tank fluid temperature
$T_{in}$	Inlet fluid temperature
$T_h$	Heating jacket temperature
$C_p$	Specific heat capacity of the tank fluid
$U$	Overall heat transfer coefficient
$A$	Heat transfer area
$Q_h$	Heat transfer from the heating jacket to the tank fluid
$\rho_f$	Fluid density
NSPC	Nonlinear Subspace Predictive Control
GA	Genetic Algorithms
BLS	Broad Learning System
LWPR	Locally Weighted Projection Regression
IAE	Integral of Absolute Error
RMPLS	Recursive Modified Partial Least Squares
SFOA	Starfish optimization algorithm
AO	Aquila Optimizer
HBA	Honey Badger Algorithm
GCRA	Greater Cane Rat Algorithm
PID	Proportional-Integral-Derivative
2DOF-PIDA	Two Degrees of Freedom-PID Acceleration
CSTH	Continuously Stirred Tank Heater
2DoF	Two-Degree-of-Freedom
ANN	Artificial Neural Network
SPID	Standard Proportional-Integral-Derivative

The control of nonlinear processes poses significant challenges due to their complex dynamics, inherent instabilities, and susceptibility to external disturbances<sup>1</sup>. Among such systems, the continuous stirred-tank heater (CSTH) serves as a classical benchmark for testing control strategies<sup>2</sup>, particularly in temperature regulation, where precise and robust control is crucial. This motivates the exploration of advanced control methods capable of addressing the unique nonlinearities and dynamic behaviors of CSTH processes while overcoming the limitations of conventional approaches.

Conventional control strategies, such as proportional-integral-derivative (PID) controllers and their variations, have been widely applied in industrial applications due to their simplicity and reliability<sup>3</sup>. These

controllers, including two-degrees-of-freedom (2DOF) PID schemes<sup>4</sup>, have demonstrated considerable success in achieving satisfactory performance for linear or mildly nonlinear systems. However, as highlighted in the literature, traditional methods often fail to deliver optimal results in highly nonlinear environments like CSTD. This shortfall emphasizes the need for optimization techniques that can refine controller parameters and improve overall system performance<sup>5</sup>.

Recent advancements in metaheuristic algorithms have addressed the shortcomings of traditional tuning methods by offering robust solutions for highly nonlinear optimization problems<sup>6</sup>. Bio-inspired algorithms, such as the starfish optimization algorithm (SFOA)<sup>7</sup>, greater cane rat algorithm (GCRA)<sup>8</sup>, honey badger algorithm (HBA)<sup>9</sup>, and aquila optimizer (AO)<sup>10,11</sup>, have shown remarkable potential in achieving global optimal solutions. These techniques strike a fine balance between exploration and exploitation phases, making them suitable for complex control tasks. Among them, SFOA has demonstrated superior convergence rates and robustness, particularly in applications involving nonlinear constraints. Yet, the specific impact of these algorithms in CSTD temperature control systems remains underexplored.

Temperature regulation in CSTD systems has long been a critical challenge in process industries due to the highly nonlinear and multivariable nature of these systems. However, almost no significant studies has been performed over the years to improve performance and robustness in CSTD processes. In a study conducted by Gao, et al.<sup>12</sup> data-driven predictive control strategy utilizing recursive modified partial least squares (RMPLS) and locally weighted projection regression (LWPR) was introduced. This method effectively regressed local linear models to adapt to dynamic process conditions, significantly outperforming traditional model-free adaptive control methods in predictive accuracy and robustness. Mahmood and Nawaf<sup>13</sup> analyzed the PID-cascade control architecture for CSTD systems, highlighting its strengths in disturbance rejection and setpoint tracking. However, the study emphasized its limitations in handling strong nonlinearities, particularly under varying operational conditions, necessitating advanced controller designs. Tao, et al.<sup>14</sup> proposed a broad learning system (BLS)-aided predictive control strategy to address computational challenges associated with neural network-based controllers. The approach reduced computational complexity while maintaining high predictive accuracy and control precision, making it a viable choice for real-time CSTD applications.

In a complementary direction, Wu and Yang<sup>15</sup> developed a Nonlinear subspace predictive control (NSPC) framework incorporating locally weighted projection regression (LWPR). This method addressed nonlinear dynamics effectively by constructing localized models, yielding enhanced tracking and predictive performance in CSTD benchmarks. Several studies have also focused on the role of metaheuristic optimization in enhancing CSTD control. For instance, Dhanasekar and Vijayachitra<sup>2</sup> explored hybrid optimization techniques, combining genetic algorithms (GA), pattern search, and Fmin search to optimize PID controller parameters. Their approach improved system stability and reduced steady-state error in CSTD processes. Similarly, Hashim, et al.<sup>9</sup> introduced the HBA, demonstrating its efficiency in balancing exploration and exploitation to achieve optimal control in nonlinear systems.

Artificial neural network (ANN)-based control strategies have also gained traction. Ang, et al.<sup>16</sup> implemented ANN controllers for CSTD systems, leveraging their adaptability to nonlinear dynamics and disturbance rejection. The study demonstrated the potential of ANN-based controllers to handle system complexities more effectively than traditional methods. Further, Ahmed, et al.<sup>17</sup> investigated advanced PID tuning methods, including Ziegler-Nichols and fuzzy logic approaches, highlighting their limitations under dynamic conditions and proposing enhancements to improve performance in CSTD applications. Finally, Li and Jiang<sup>18</sup> demonstrated the use of CSTD as an educational platform for process control. They showcased practical applications of PID and cascade controllers, emphasizing the importance of integrating theoretical knowledge with real-world system dynamics. Table 1 presents a review of key contributions from the literature to establish the foundation and identify the gaps addressed in this study.

Despite the significant advancements highlighted above, there remains a gap in the integration of novel metaheuristic algorithms, such as the SFOA, with advanced controllers like the 2DOF-PIDA. To address these gaps, this paper proposes a novel control strategy that combines the 2DOF-PIDA controller with SFOA. The 2DOF-PIDA controller introduces enhanced flexibility for decoupling setpoint tracking and disturbance rejection, while SFOA optimizes the controller parameters to ensure optimal performance. This seamless integration provides a promising framework for overcoming the challenges associated with temperature regulation in CSTD processes, setting the stage for its validation through simulation and comparative analysis.

Article	Method	Theory	Findings
Ref. <sup>13</sup>	Cascade PID control analysis for nonlinear CSTD processes	Combination of PID and cascade architecture	Effective disturbance rejection but limited performance in nonlinear conditions
Ref. <sup>14</sup>	BLS integrated with predictive control	Broad Learning for reduced computation and higher precision	Reduced computational complexity and improved precision in CSTD applications
Ref. <sup>2</sup>	Hybrid optimization using GA, Pattern Search, and Fmin Search	Combining metaheuristics for advanced PID tuning	Improved stability and reduced errors in CSTD control
Ref. <sup>9</sup>	Metaheuristic optimization with HBA	Exploration and exploitation balance in metaheuristics	Efficient optimization for nonlinear CSTD tuning
Ref. <sup>18</sup>	Implementation of PID and cascade control in education	Practical teaching applications for nonlinear control	Strengthened practical understanding of control strategies

**Table 1.** Overview of the previous research.

The paper is organized as follows: section “[Modeling of CSTH temperature control system](#)” introduces the mathematical modeling of the CSTH system. Section “[Mathematical model of starfish optimization algorithm \(SFOA\)](#)” presents the optimization using the SFOA algorithm. Additionally, in this section, the SFOA optimization technique is discussed, emphasizing its effectiveness in parameter tuning. Section “[Novel temperature control design approach for CSTH process](#)” focuses on the implementation of the 2DOF-PIDA controller for the continuously stirred tank heater, optimized via SFOA to improve stability and system response. Section “[Simulation results](#)” provides simulation results and a detailed comparison with other widely used controllers and meta-heuristic optimization techniques. Lastly, section “[Conclusion and future work](#)” summarizes the key conclusions and suggests future research directions.

### Modeling of CSTH temperature control system

The CSTH plays a vital role in industrial temperature control applications. It functions by maintaining a consistent heating process within a tank, utilizing a jacketed heating mechanism to precisely regulate temperature levels. The CSTH system integrates complex dynamic processes, such as fluid flow, heat transfer, and control strategies, which are represented through nonlinear mathematical models. Achieving accurate modeling and parameter optimization is crucial to ensuring the system’s efficiency and effective performance. Figure 1 illustrates the general schematic of the CSTH system<sup>19,20</sup>.

The behavior of the CSTH system is governed by fundamental principles, including mass balance, energy balance, and heat transfer. The mass balance equation upholds the conservation of mass throughout the system<sup>21,22</sup>:

$$\frac{dM}{dt} = \rho_f Q_{in} - \rho_f Q_{out} \quad (1)$$

In the mass balance equation,  $M$  denotes the mass of the fluid within the tank, while  $\rho_f$  represents the fluid density. The terms  $Q_{in}$  and  $Q_{out}$  correspond to the inlet and outlet flow rates, respectively.

The energy balance equation characterizes the dynamic changes in the fluid temperature inside the tank, taking into account both heat transfer mechanisms and flow dynamics. This equation provides insights into how thermal energy is distributed and conserved within the system, ensuring efficient temperature regulation<sup>21</sup>:

$$\frac{d(T_t M)}{dt} = \rho_f C_p Q_{in} (T_{in} - T_t) + UA (T_h - T_t) \quad (2)$$

In the energy balance equation, the parameters are defined as follows:  $T_t$  represents the temperature of the fluid inside the tank while  $T_{in}$  and  $T_h$  denote the inlet fluid temperature and the heating jacket temperature, respectively. The specific heat capacity of the tank fluid is denoted by  $C_p$ , whereas  $U$  represents the overall heat transfer coefficient, and  $A$  is the heat transfer area.

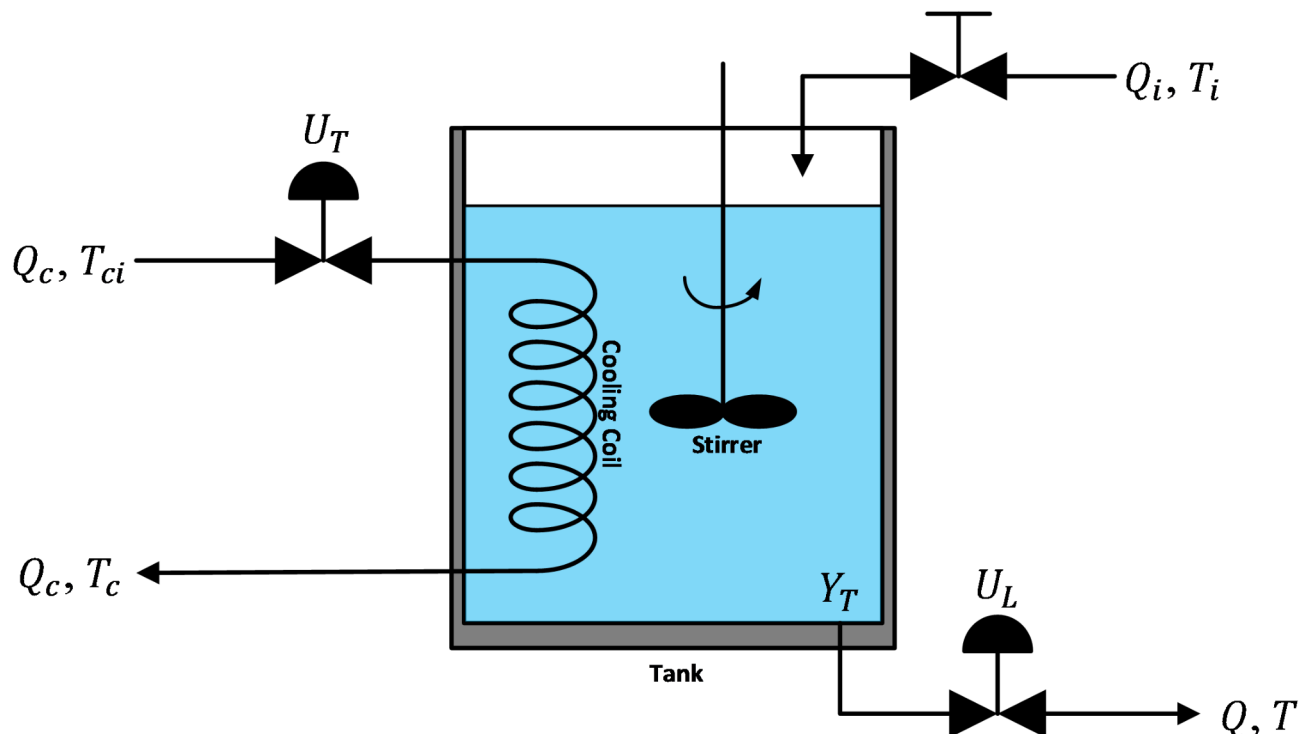


**Fig. 1.** Schematic representation of CSTH control system.

The heat transfer equation quantitatively measures the thermal energy transferred from the heating jacket to the tank fluid, ensuring effective temperature regulation and process stability within the system. The heat transfer equation quantifies the amount of thermal energy transferred from the heating jacket to the fluid tank, ensuring efficient temperature regulation within the system. It is expressed as<sup>13</sup>:

$$Q_h = UA(T_h - T_t) \quad (3)$$

This equation highlights the dependence of heat transfer on the temperature difference between the heating jacket and the tank fluid, as well as the efficiency of the heat exchange surface.

### Transfer function model of CSTH

To develop the transfer function model of the CSTH system, we apply the Laplace transform to the energy balance equation:

$$(MC_{PS} + \rho_f C_P Q_{in}) T_t(s) = \rho_f C_P Q_{in} T_t(s) + UAT_h(s) \quad (4)$$

Rearranging for  $T_t(s)$  :

$$T_t(s) = \frac{1}{MC_{PS} + \rho_f C_P Q_{in}} \times [\rho_f C_P Q_{in} T_t(s) + UAT_h(s)] \quad (5)$$

Defining the time constant  $\tau = \frac{M}{\rho_f Q_{in}}$ , the transfer function relating the heater power  $Q_h(s)$  to the tank temperature  $T_t(s)$  is:

$$G(s) = \frac{T_t(s)}{Q_h(s)} = \frac{1}{\tau s + 1} \quad (6)$$

Similarly, the transfer function from the inlet temperature  $T_{in}(s)$  to the output temperature is:

$$G(s) = \frac{T_t(s)}{T_{in}(s)} = \frac{\rho_f C_P Q_{in}}{\tau s + 1} \quad (7)$$

This transfer function model effectively represents the dynamic behavior of the CSTH system, capturing the heat transfer and flow characteristics.

### Comprehensive parameters defining the CSTH control system

The parameters listed in Table 2 thoroughly describe the physical, thermal, and control characteristics of the CSTH process. These parameters are essential for accurately modeling, analyzing, and controlling system behavior, ensuring optimal performance and stability under varying operational conditions<sup>19,20</sup>.

#### Fluid properties

The tank fluid has a density ( $\rho$ ) of 1200 kg/m<sup>3</sup> and a specific heat capacity ( $C_p$ ) of 4190 J/(kg°C), both of which are crucial for energy and mass balance equations. Similarly, the heating fluid possesses a density ( $\rho_c$ ) of 800 kg/m<sup>3</sup> and a specific heat capacity ( $C_{pc}$ ) of 2400 J/(kg°C), enabling precise modeling of heat transfer between the heating jacket and the tank fluid.

#### Geometric dimensions

The design dimensions of the tank and heating jacket significantly influence heat transfer efficiency and fluid dynamics. The tank features a diameter ( $D$ ) of 0.3 m, an internal cross-sectional area ( $A$ ) of 0.0225 $\pi$  m<sup>2</sup>, and a wall height  $H_t$  of 0.9 m. The heating jacket is characterized by a heat transfer area  $A_c$  of 0.2025 $\pi$  m<sup>2</sup>, a width  $W_c$  of 0.02 m, a height  $H_c$  of 0.6 m, and a volume  $V_c$  of 0.0044 $\pi$  m<sup>3</sup>. These parameters are fundamental to evaluating heat exchange effectiveness and fluid behavior.

#### Thermal properties

The overall heat transfer coefficient ( $U$ ) of 440 J/(°C s m<sup>2</sup>) defines the system's capacity to transfer heat from the heating jacket to the tank fluid. The heating fluid inlet temperature ( $T_{ci}$ ) of 320 °C and the process fluid inlet temperature ( $T_i$ ) of 24 °C establishes the driving temperature gradient necessary for effective heat transfer.

#### Control system parameters

Key control parameters ensure accurate regulation of fluid level and temperature. The level transmitter has a gain  $K_L$  of 125%/m with a time constant ( $T_L$ ) of 2 s, while the temperature transmitter has a gain ( $K_T$ ) of 2%/°C and a time constant ( $T_T$ ) of 15 s. The level control valve features a constant ( $K_{vL}$ ) of 0.000015 and a stem constant ( $K_{xL}$ ) of 0.01%. Similarly, the temperature control valve has a constant ( $K_{vT}$ ) of 0.000003 and a stem constant  $K_{xT}$  of 0.01%. The valve time constants are  $T_{vL} = 3$  s and  $T_{vT} = 5$  s, respectively.

#### Fluid dynamics parameters

The nominal tank inlet flow rate ( $Q_i$ ) of 0.0007 m<sup>3</sup>/s, and the pipe flow resistance ( $R_c$ ) of the heating fluid system is 55 × 10<sup>6</sup> kPa/(m<sup>3</sup>/s)<sup>2</sup>. The heating fluid pump discharge pressure ( $P_{cp}$ ) is 414 kPa, while the return pressure ( $P_{cr}$ ) is 138 kPa, ensuring appropriate pressure conditions for system operation.

Parameter	Value	Unit
$\rho$ (tank fluid density)	1200	kg/m <sup>3</sup>
$\rho_c$ (heating fluid density)	800	kg/m <sup>3</sup>
$D$ (tank diameter)	0.3	m
$A$ (tank inside section area)	$0.0225 \times \pi$	m <sup>2</sup>
$A_c$ (jacket heat transfer area)	$0.2025 \times \pi$	m <sup>2</sup>
$C_p$ (tank fluid heat capacity)	4190	J/(kg°C)
$C_{pc}$ (heating fluid heat capacity)	2400	J/(kg°C)
$g$ (gravity constant)	9.8	m/s <sup>2</sup>
$K_L$ (level transmitter gain)	125	%m
$K_T$ (temperature transmitter gain)	2	%/°C
$K_{vL}$ (level control valve constant)	0.000015	-
$K_{vT}$ (temperature control valve constant)	0.000003	-
$K_{wL}$ (level control valve stem constant)	0.01	%
$K_{wT}$ (temperature control valve stem constant)	0.01	%
$Q_i$ (normal tank inlet fluid flow rate)	0.0007	m <sup>3</sup> /s
$T_i$ (fluid inlet temperature)	24	°C
$T_{ci}$ (heating fluid inlet temperature)	320	°C
$T_{sp}$ (temperature controller set-point)	38	°C
$T_L$ (level transmitter time constant)	2	s
$T_T$ (temperature transmitter time constant)	15	s
$T_{vL}$ (level control valve time constant)	3	s
$T_{vT}$ (temperature control valve time constant)	5	s
$P_{cp}$ (heating fluid pump discharge pressure)	414	kPa
$P_{cr}$ (heating fluid system return pressure)	138	kPa
$R_c$ (heating system pipe nominal flow resistance)	$55 \times 10^6$	kPa/(m <sup>3</sup> /s) <sup>2</sup>
$R_{vT}$ (temperature control valve rangeability)	50	-
$U$ (overall heat-transfer coefficient)	440	J/(°Csm <sup>2</sup> )
$V_c$ (heat jacket volume)	$0.0044 \times \pi$	m <sup>3</sup>
$W_c$ (heating jacket wide)	0.02	m
$H_c$ (heating jacket height)	0.6	m
$H_t$ (tank wall height)	0.9	m
$H_{sp}$ (level controller set-point)	0.7	m

**Table 2.** Definition of parameters in CSTH system<sup>19,20</sup>.

#### Control set-points

The system operates with a temperature controller set-point ( $T_{sp}$ ) of 38 °C and a level controller set-point ( $H_{sp}$ ) of 0.7 m, defining the desired operational targets for the CSTH system.

#### Additional parameters

The gravity constant ( $g$ ) of 9.8 m/s<sup>2</sup> is critical for fluid behavior calculations within the tank. Moreover, the temperature control valve rangeability ( $R_{vT}$ ) of 50 provides flexibility in adjusting flow rates to meet operational demands. Collectively, these parameters establish a robust foundation for the design, simulation, and optimization of the CSTH system, ensuring its efficiency and stability under diverse operational conditions.

#### Murrill-tuned PID control method

The standard PID controller used in Murrill's tuning method is represented as<sup>23</sup>:

$$G_c(s) = K_p \left( 1 + \frac{1}{T_i s} + T_d s \right) \quad (8)$$

where,  $K_p$ ,  $T_i$  and  $T_d$  are proportional gain, integral time constant and derivative time constant respectively.

**Tuning formulas for PID controller** For moderate dead-time systems, where  $0.5 \leq \frac{\theta}{\tau} \leq 1.5$ , the following empirical tuning rules apply:

$$K_c = \frac{1.2}{K_P} \left( \frac{\tau}{\theta} \right), \quad T_i = 2\theta, \quad T_d = 0.5\theta \quad (9)$$

These formulas ensure a well-balanced response with minimal oscillations while maintaining a trade-off between stability and performance.

#### Standard PID (SPID) controller and Murrill-tuned control method

The standard proportional-integral-derivative (SPID) controller is a widely utilized control strategy in industrial applications, providing effective regulation of system dynamics by combining proportional, integral, and derivative actions. The transfer function of the SPID controller serves as a mathematical representation of the system's dynamic behavior in the frequency domain, allowing for the analysis of stability and performance characteristics. The general expression of the transfer function incorporates the proportional gain, which directly responds to the current error; the integral gain, which accumulates past errors to eliminate steady-state deviations; and the derivative gain, which anticipates future errors to improve stability. Transfer function of the SPID controller is expressed as follows<sup>24</sup>:

$$C_{SPID}(s) = \frac{U(s)}{E(s)} = K_p \left( 1 + \frac{1}{T_i s} + \frac{T_d s}{\alpha_d T_d s + 1} \right) \quad (10)$$

In this study<sup>19</sup>, the Murrill-tuned SPID control method was applied to a Csth system, demonstrating its effectiveness in temperature regulation. Figure 2 refers to the time response of the Murrill-tuned SPID-controlled Csth temperature control system. The system's setpoint ( $Y_{T,sp}(t)$ ) was increased from 76 to 81%, and the corresponding response was analyzed to evaluate the controller's performance.

The observed results illustrate the controller's ability to accurately track setpoint changes while maintaining stability and minimizing overshoot. The Murrill tuning method is critical in refining the PID parameters to balance response speed and system stability, ensuring optimal performance under varying operating conditions. The time response characteristics obtained from the implementation highlight the practical benefits of using this tuning approach in industrial temperature control applications.

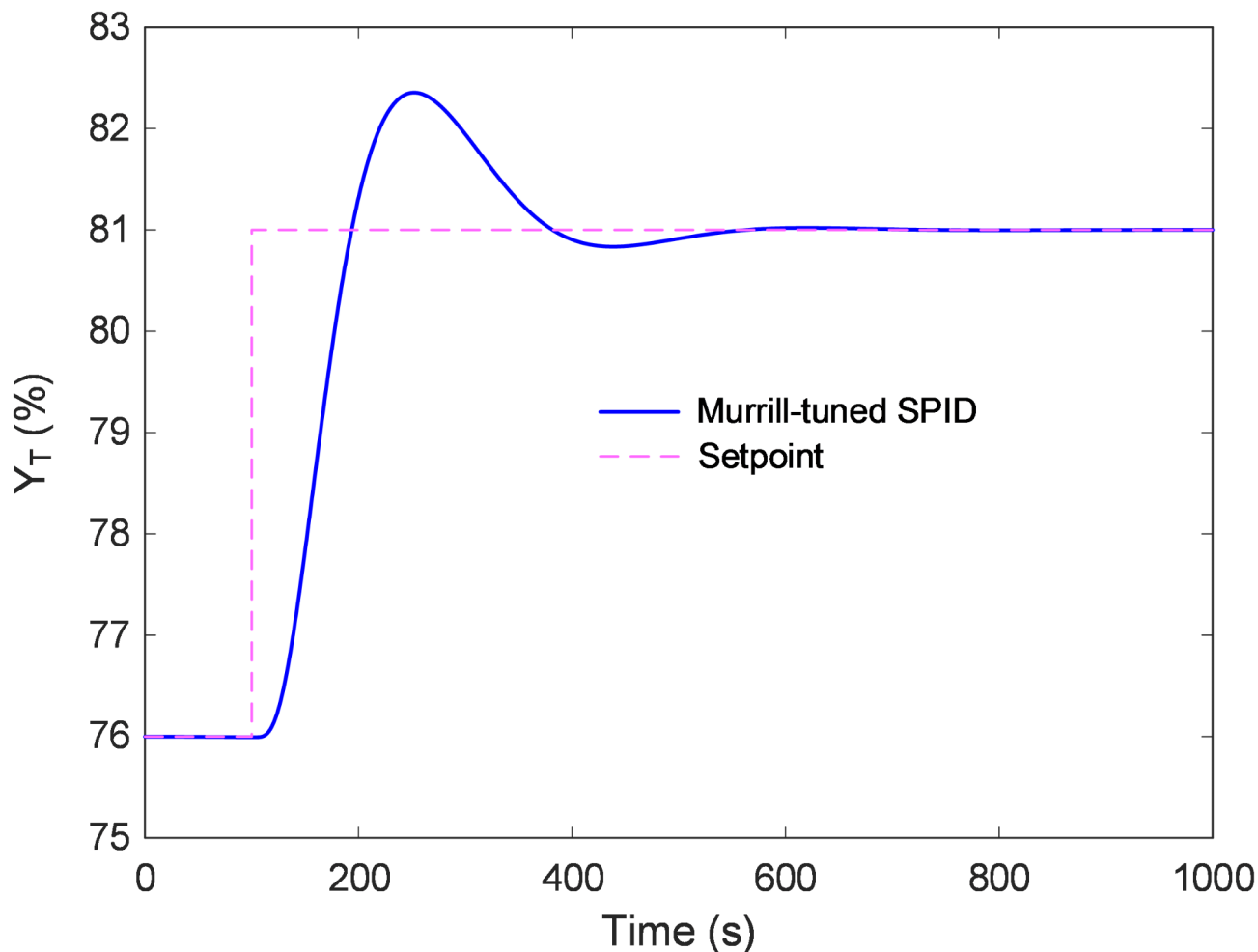


**Fig. 2.** Time response of Murrill-tuned SPID controlled Csth temperature control system.

## Mathematical model of starfish optimization algorithm (SFOA)

The starfish optimization algorithm (SFOA) is a bio-inspired metaheuristic approach designed to solve optimization problems by imitating the natural behaviors of starfish, including exploration, preying, and regeneration. The algorithm aims to balance exploration, which ensures a thorough search of the solution space, and exploitation, which refines the search towards the optimal solution. In the initialization phase, the positions of the starfish, representing candidate solutions, are randomly generated within the defined search space. This can be expressed mathematically as:

$$X_{ij} = l_j + (u_j - l_j) \cdot r, \quad r \in (1, 0) \quad (11)$$

where  $X_{ij}$  represents the position of the  $i_{th}$  starfish in the  $j_{th}$  dimension, and  $l_j$ ,  $u_j$  are the lower and upper bounds of the search space, respectively. The exploration phase of SFOA employs a hybrid search pattern that depends on the problem's dimensionality. For high-dimensional problems where  $D > 5$ , the search strategy utilizes a five-dimensional approach inspired by the movement of the starfish's arms. The position update formula in this case is:

$$\begin{cases} Y_{i,p}^{(t)} = X_{i,p}^{(t)} + \alpha \left( X_{best,p}^{(t)} - X_{i,p}^{(t)} \right) \times \cos(\theta) & r \leq 0.5 \\ Y_{i,p}^{(t)} = X_{i,p}^{(t)} - \alpha \left( X_{best,p}^{(t)} - X_{i,p}^{(t)} \right) \times \sin(\theta) & r > 0.5 \end{cases} \quad (12)$$

where  $\alpha$  is defined as  $(2r - 1)\pi$  and  $\theta$  is calculated as  $\frac{\pi}{2} \left( \frac{T}{T_{max}} \right)$ . In contrast, for problems with  $D \leq 5$ , a unidimensional search pattern is applied, where the position update is given by:

$$Y_{i,q}^{(t)} = E^t X_{i,p}^{(t)} + A_1 \left( X_{k_1,p}^{(t)} - X_{i,p}^{(t)} \right) + A_2 \left( X_{k_2,p}^{(t)} - X_{i,p}^{(t)} \right) \quad (13)$$

In this equation,  $E^t$  represents the energy of the starfish, calculated as  $\left( \frac{T_{max} - T}{T_{max}} \right) \cos(\theta)$ , ensuring a gradual reduction of exploration over time. In the exploitation phase, SFOA introduces mechanisms inspired by starfish preying and regeneration behaviors to refine the search process. The preying behavior employs a two-directional search strategy, which adjusts the starfish positions based on their proximity to the best-known solution. This is formulated as:

$$Y_i^{(t)} = X_i^{(t)} + r_1 d_{m1} + r_2 d_{m2} \quad (14)$$

where the distances  $d_m$  are calculated between the global best solution and the individual starfish. The regeneration phase further improves convergence by gradually adjusting the position of the last starfish in the population using the following formula:

$$Y_i^{(t)} = \exp\left(-\frac{T \times N}{T_{max}}\right) \times X_i^{(t)} \quad (15)$$

To ensure feasible solutions, any position that exceeds the search space boundaries is adjusted as follows:

$$X_i^{(t+1)} = \begin{cases} Y_i^{(t)} & l \leq Y_i^{(t)} \leq u \\ l & Y_i^{(t)} < l \\ u & Y_i^{(t)} > u \end{cases} \quad (16)$$

The algorithm runs iteratively until a termination criterion, typically the maximum number of iterations  $T_{max}$ , is reached. Once the optimization process is complete, the best-found solution is returned. Figure 3 presents the flowchart of SFOA.

## Novel temperature control design approach for Csth process

### 2DOF-PIDA controller

The 2DOF-PIDA controller represents an advanced control technique that improves system dynamic performance through acceleration feedback integration with standard proportional integral derivative elements. The 2DOF-PIDA controller offers greater adaptability and stability than standard PID controllers, resulting in better performance in disturbance rejection and reference tracking. The transfer function of the proposed 2DOF-PIDA controller can be expressed as follows:

$$U(s) = K_p \left( \beta \times R(s) - Y(s) + \frac{1}{T_{is}} [R(s) - Y(s)] + \frac{T_{as}}{\alpha_d T_{ds} + 1} [\gamma \times R(s) - Y(s)] + \left( \frac{T_{as}}{\alpha_a T_{as} + 1} \right)^2 [R(s) - Y(s)] \right) \quad (17)$$

The block diagram of the 2DOF-PIDA controller is illustrated in Fig. 4, consists of two distinct feedback loops. Two distinct feedback loops form the 2DOF-PIDA controller block diagram shown in Fig. 4, including a primary feedback loop that controls system output and an auxiliary loop that adds control action through acceleration feedback. The control system benefits from better handling of different system dynamics and external disturbances due to its dual-loop structure.

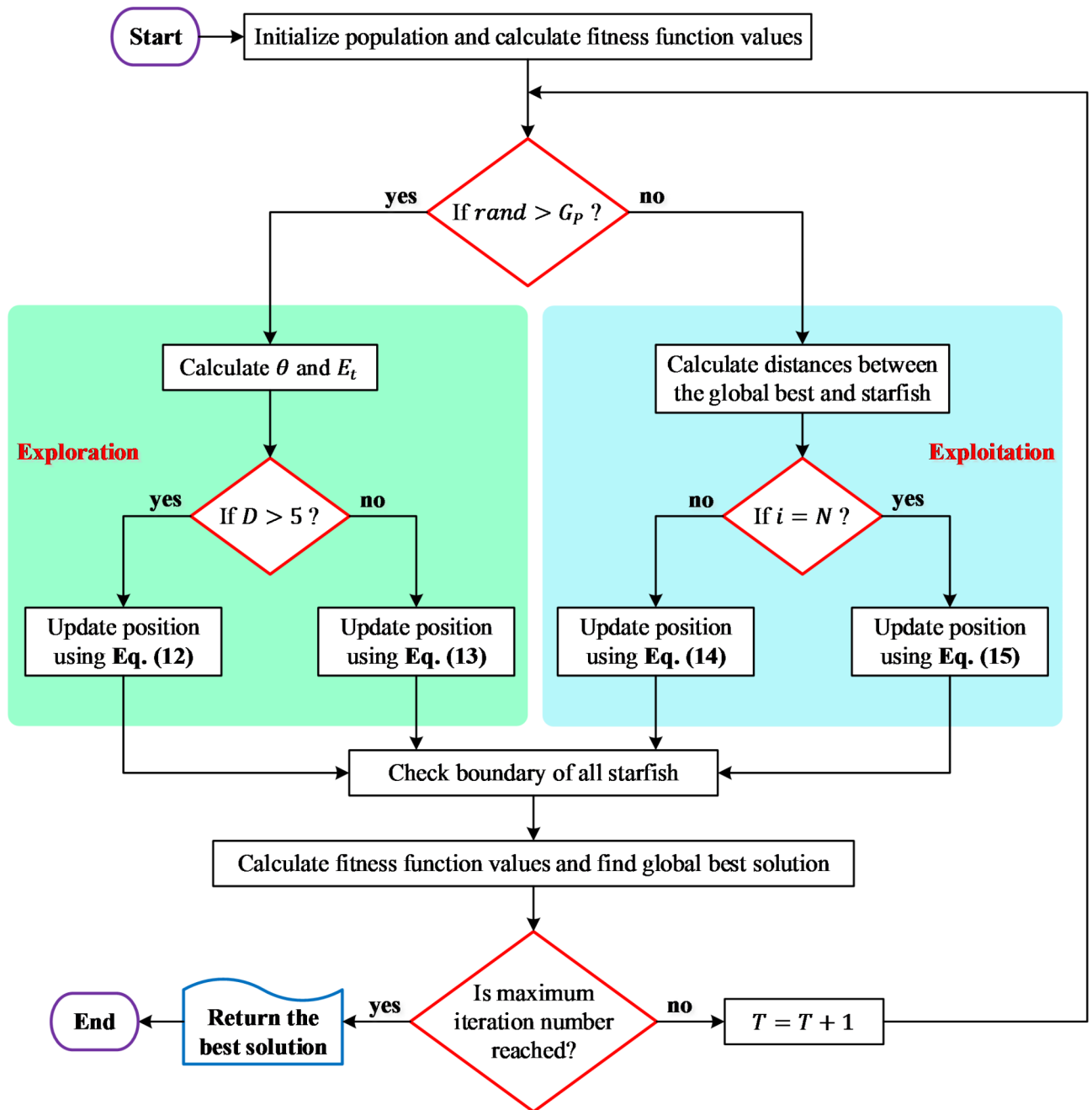


Fig. 3. Flowchart of SFOA.

### Definition of novel cost function

The new cost function presented in this investigation seeks to improve control performance by reducing the deviation between the setpoint signal and temperature transmitter output throughout a set simulation interval. This study analyzes the system response characteristics over a complete 1000s simulation time. The cost function combines mathematical formulations with key performance indices like overshoot and steady-state error to meet set control objectives. The cost function can be expressed as follows<sup>25</sup>:

$$F_{IAE} = \int_0^{t_{final}} |e(t)| dt \tag{18}$$

where,  $e(t) = Y_{T,sp}(t) - Y_T(t)$  is an error between the setpoint signal and the temperature transmitter output,  $t_{final}$  is simulation time. The proposed optimization approach aims to minimize the cost function (CF), which is designed to balance between tracking accuracy and normalized overshoot. The cost function is mathematically defined as:

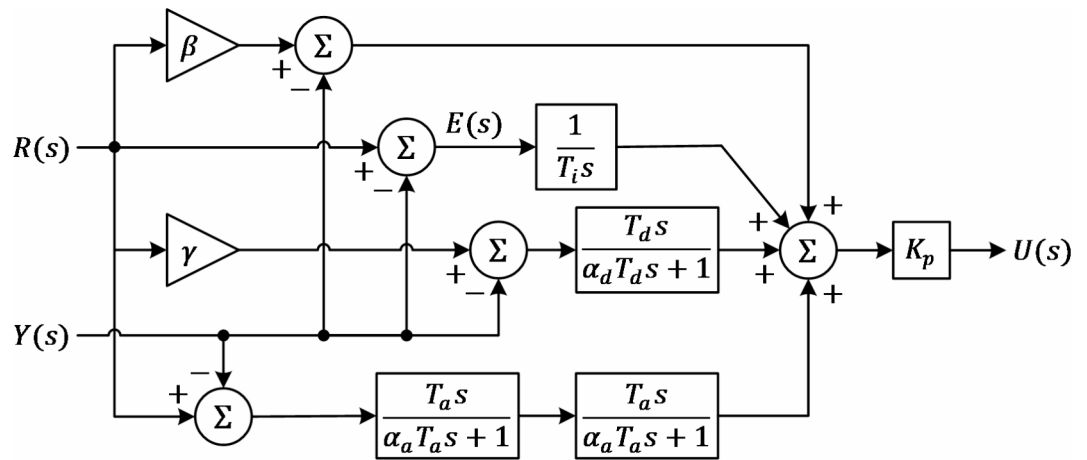


Fig. 4. Block diagram of 2DOF-PIDA controller.

Parameters	$K_p$	$T_i$	$T_d$	$\alpha_d$	$\beta$	$\gamma$	$T_a$	$\alpha_a$
Upper bound	20	200	100	0.25	2	10	25	0.25
Lower bound	1	20	10	0.05	0.5	0.1	10	0.05

Table 3. Upper and lower parameter bounds.

$$CF = \varphi \times F_{IAE} + (1 - \varphi) \times O_{s, norm} \tag{19}$$

Scaling factor  $\varphi = 0.05$ , which prioritizes the contribution of  $F_{IAE}$  in the cost function while assigning a smaller weight to  $O_{s, norm}$ . In addition,  $O_{s, norm}$  is normalized percent overshoot, which measures how much the system output exceeds the desired setpoint. To ensure the practicality and feasibility of the optimization results, the control parameters are constrained within the bounds specified in Table 3, where  $K_p, T_i, T_d, \alpha_d, \beta, \gamma, T_a$  and  $\alpha_a$  represent proportional gain, integral time constant, derivative time constant, derivative filter coefficient, the weighting factor for proportional action, scaling parameter, acceleration time constant, and acceleration filter coefficient, respectively.

### Working mechanism of proposed SFOA-tuned 2DOF-PIDA control method for CSTH process

The control method presented combines the SFOA with a 2DOF-PIDA controller to maintain stable temperature regulation in CSTH operations. Figure 5 shows the detailed block diagram of the control strategy while the SFOA optimization algorithm adjusts the 2DOF-PIDA controller parameters in real-time to improve performance under various operational conditions and tackle non-linearities and uncertainties in the CSTH process.

The 2DOF-PIDA controller separates tuning settings to manage setpoint tracking while independently handling disturbance rejection. The division between functions reduces the trade-offs that exist in traditional single-degree-of-freedom controllers. SFOA achieves optimal parameter adjustment, which reduces overshooting and enhances system stability through effective exploration and exploitation of the parameter space using swarm intelligence.

### Comparison with Murrill-tuned SPID control method

The SFOA-tuned 2DOF-PIDA controller demonstrates better performance compared to the conventional Murrill-tuned standard proportional-integral-derivative (SPID) controller according to a comparative analysis. The dynamic performance enhancement achieved by the SFOA-tuned 2DOF-PIDA control method is demonstrated through time response characteristics in Fig. 6. The performance of the proposed SFOA-tuned 2DOF-PIDA controller is evaluated using key normalized time response metrics, including the normalized rise time ( $t_{rise, norm}$ ), normalized settling time ( $t_{set, norm}$ ), normalized percent overshoot ( $O_{s, norm}$ ), and normalized percent steady-state error ( $E_{ss, norm}$ ). These metrics provide a standardized framework for analyzing the controller's dynamic and steady-state performance.  $t_{rise, norm}$  represents the time required for the system response to increase from 10 to 90% of its final value.  $t_{set, norm}$  is defined as the time it takes for the system to settle within a  $\pm 2\%$  tolerance band around the final steady-state value.  $O_{s, norm}$  quantifies the percentage by which the response exceeds the final steady-state value during transient conditions. Finally, the  $E_{ss, norm}$  measures the deviation of the system's output from its final value at the final time.

Table 4 presents a comparative analysis of time response metrics, highlighting the performance differences among the evaluated methods. The rise time ( $t_{rise, norm}$ ) of the SFOA-tuned 2DOF-PIDA controller is significantly reduced, achieving a value of 50.6027 s compared to the 54.7109 s recorded for the Murrill-tuned SPID controller. This reduction reflects the proposed controller's ability to respond more quickly to input changes.

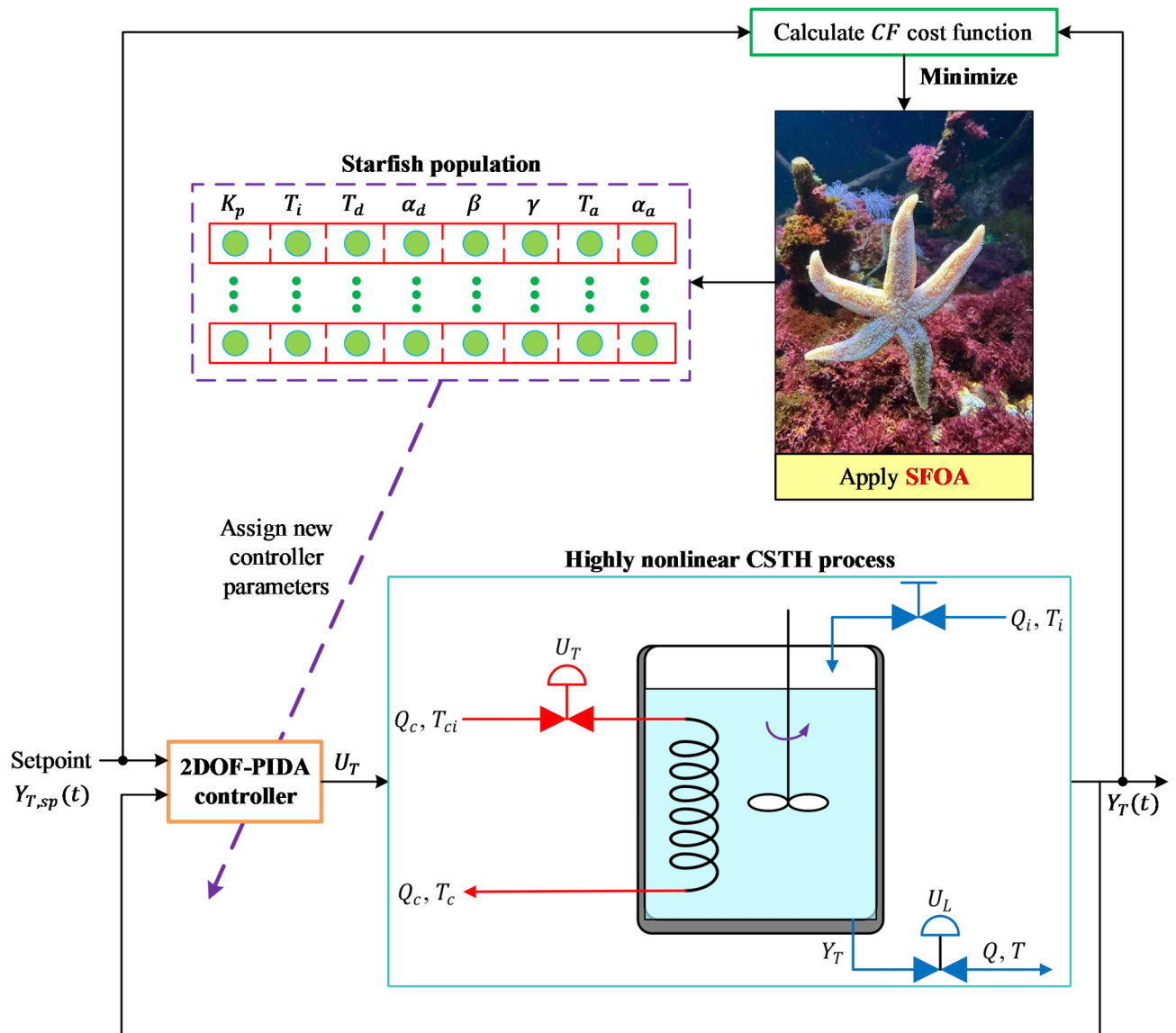


**Fig. 5.** Detailed block diagram of SFOA-tuned 2DOF-PIDA control method for CSTH temperature control system.

Furthermore, the settling time ( $t_{set, norm}$ ) shows a dramatic improvement, decreasing to 192.5837 s, which is markedly faster than the 492.3235 s required by the SPID controller. In terms of stability, the percent overshoot ( $O_{s, norm}$ ) is minimized to an almost negligible value of 0.0183%, a stark contrast to the 27.1128% observed in the SPID controller. This reduction indicates that the proposed controller excels in mitigating transient responses and maintaining system stability. Additionally, the steady-state error ( $E_{ss, norm}$ ) is reduced to  $4.2105 \times 10^{-5}$ , showcasing an exceptional level of precision, far surpassing the SPID controller's error of 0.0057%. The SFOA-tuned 2DOF-PIDA controller shows improved performance through faster response times along with enhanced stability and accuracy, as demonstrated by these results. The advanced control approach proves appropriate for CSTH system temperature regulation because significant performance metric enhancements validate its effectiveness.

### Simulation results

The statistical verification of the SFOA was conducted to validate its performance against several recent metaheuristic algorithms, including the greater cane rat algorithm (GCRA)<sup>8</sup>, the mantis search algorithm (MSA)<sup>26</sup>, the honey badger algorithm (HBA)<sup>9</sup> and the Aquila optimizer AO<sup>10</sup>. All algorithms were evaluated under identical conditions with a population size of  $N_{ps} = 40$  and a maximum iteration limit of  $T_{max} = 50$ . The comparison involved 30 independent runs, using default parameter settings for all algorithms to ensure consistency and fairness.

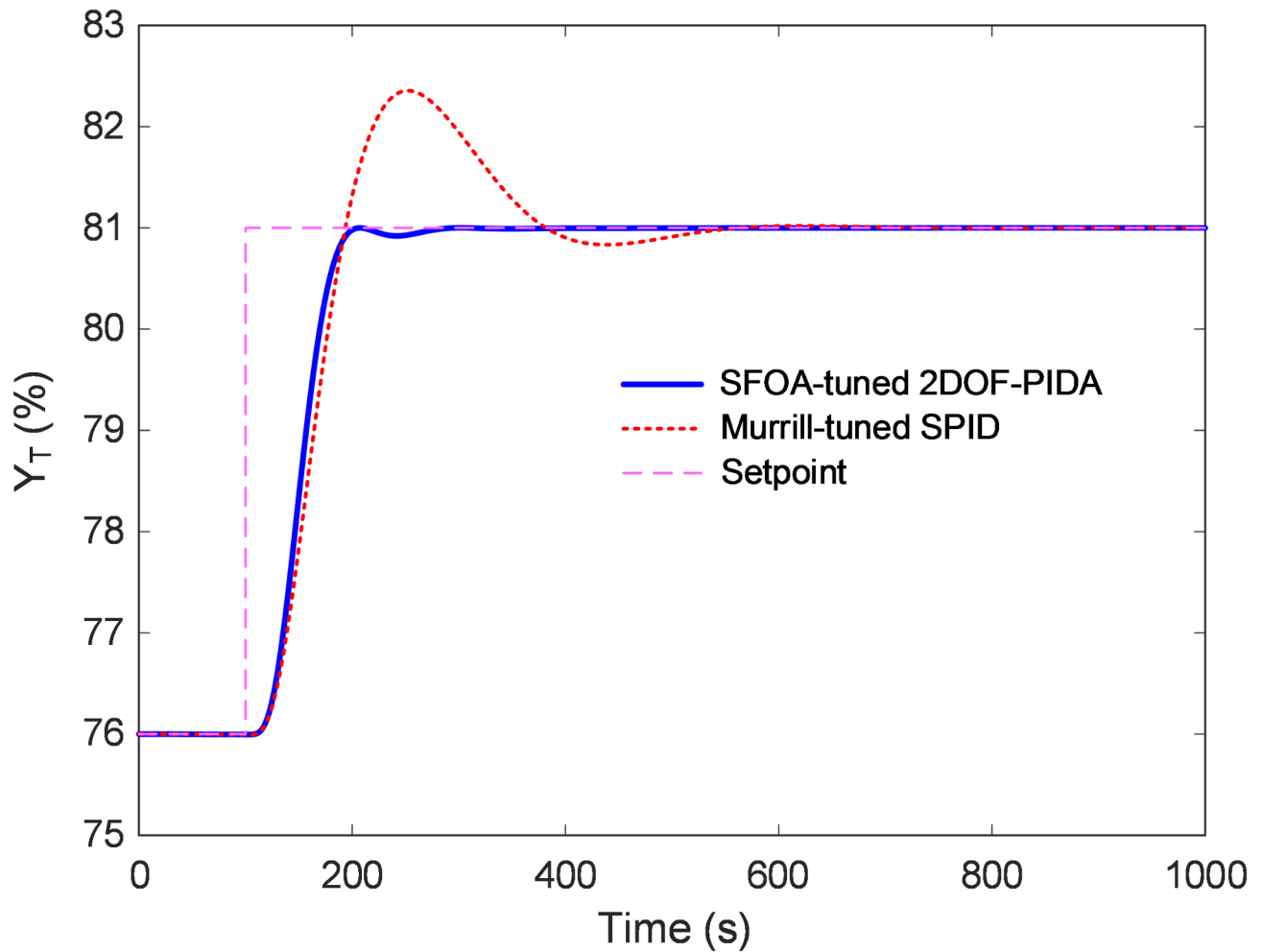


**Fig. 6.** Comparison of time responses for proposed SFOA-tuned 2DOF-PIDA and Murrill-tuned SPID control methods.

Time response metric	SFOA-tuned 2DOF-PIDA	Murrill-tuned SPID
$t_{rise,norm}$ (s)	50.6027	54.7109
$t_{set,norm}$ (s)	192.5837	492.3235
$O_s,norm$ (%)	0.0183	27.1128
$E_{ss,norm}$ (%)	4.2105E-05	0.0057

**Table 4.** Comparison of time response metrics.

### Statistical verification of SFOA

Figure 7 depicts the performance distribution of SFOA alongside other algorithms through boxplot analysis. SFOA proves to be more consistent and reliable than other algorithms in cost function minimization through its narrower interquartile range. Detailed comparisons of key performance indicators in Table 5 support the findings with precise statistical metrics.

The minimum cost function value reached by SFOA was 13.4008, surpassing all other algorithms since GCRA had 15.1542, MSA recorded 14.1271, HBA achieved 14.8383, and AO reached 14.4750. SFOA produced the lowest maximum cost function value of 14.3734 among all algorithms, which shows its ability to consistently discover near-optimal solutions. SFOA reached a median cost function value of 13.7959, which shows its dependability and ability to deliver premium solutions in multiple executions. GCRA, MSA, HBA, and AO had median values of 15.6912, 14.4627, 15.2297, and 15.0704, respectively, which were all considerably greater. The superior performance of SFOA was confirmed by its average value of 13.8253 which surpassed the results of GCRA (15.7913), MSA (14.5567), HBA (15.3380), and AO (15.0851). The calculated standard deviation of SFOA reached 0.2765, which is the lowest value when compared to other algorithms. Analysis shows that SFOA maintained the most stable performance throughout all 30 experimental runs because it had the smallest

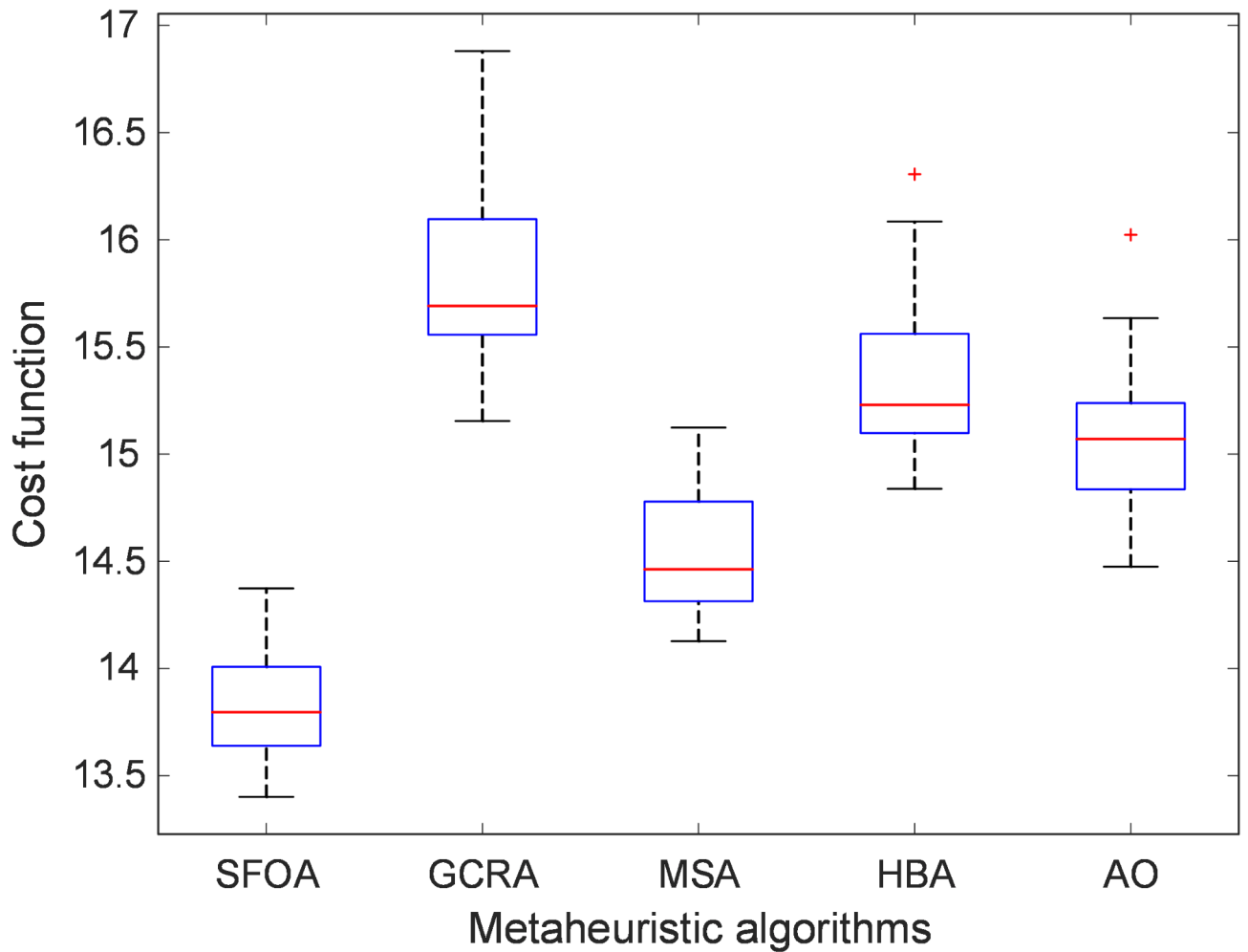


Fig. 7. Boxplot analysis of SFOA and other recent metaheuristic algorithms.

Statistical metric	SFOA	GCRA	MSA	HBA	AO
Minimum	13.4008	15.1542	14.1271	14.8383	14.4750
Maximum	14.3734	16.8804	15.1239	16.3060	16.0232
Median	13.7959	15.6912	14.4627	15.2297	15.0704
Average	13.8253	15.7913	14.5567	15.3380	15.0851
Standard deviation	0.2765	0.3864	0.2914	0.3846	0.3253

Table 5. Comparison of statistical metrics for  $CF$  cost function

variation in results. The algorithms GCRA, MSA, HBA, and AO had standard deviations measuring 0.3864, 0.2914, 0.3846, and 0.3253, respectively, which indicated these methods produced results with greater variability. The combined results show that SFOA stands out among metaheuristic algorithms because it delivers better solutions with more stability and precision in optimization problems. The findings show that SFOA functions as a robust and efficient optimization tool for complex systems.

#### Convergence curve and optimal controller parameters

The SFOA was used to evaluate the convergence behavior and optimal parameter tuning for the 2DOF-PIDA controller while comparing it to results from different metaheuristic algorithms. During the optimization process, the development of the cost function is shown in Fig. 8, demonstrating the superior convergence abilities of the SFOA. The SFOA produces lower cost values with stable performance, demonstrating its superior ability to explore the solution space and avoid suboptimal solutions in comparison, demonstrating its superior ability to explore the solution space and avoid suboptimal solutions compared to other algorithms.

In terms of computational cost, the results reveal that SFOA consistently achieves faster convergence, requiring fewer iterations to reach an optimal solution. This characteristic is particularly beneficial for real-

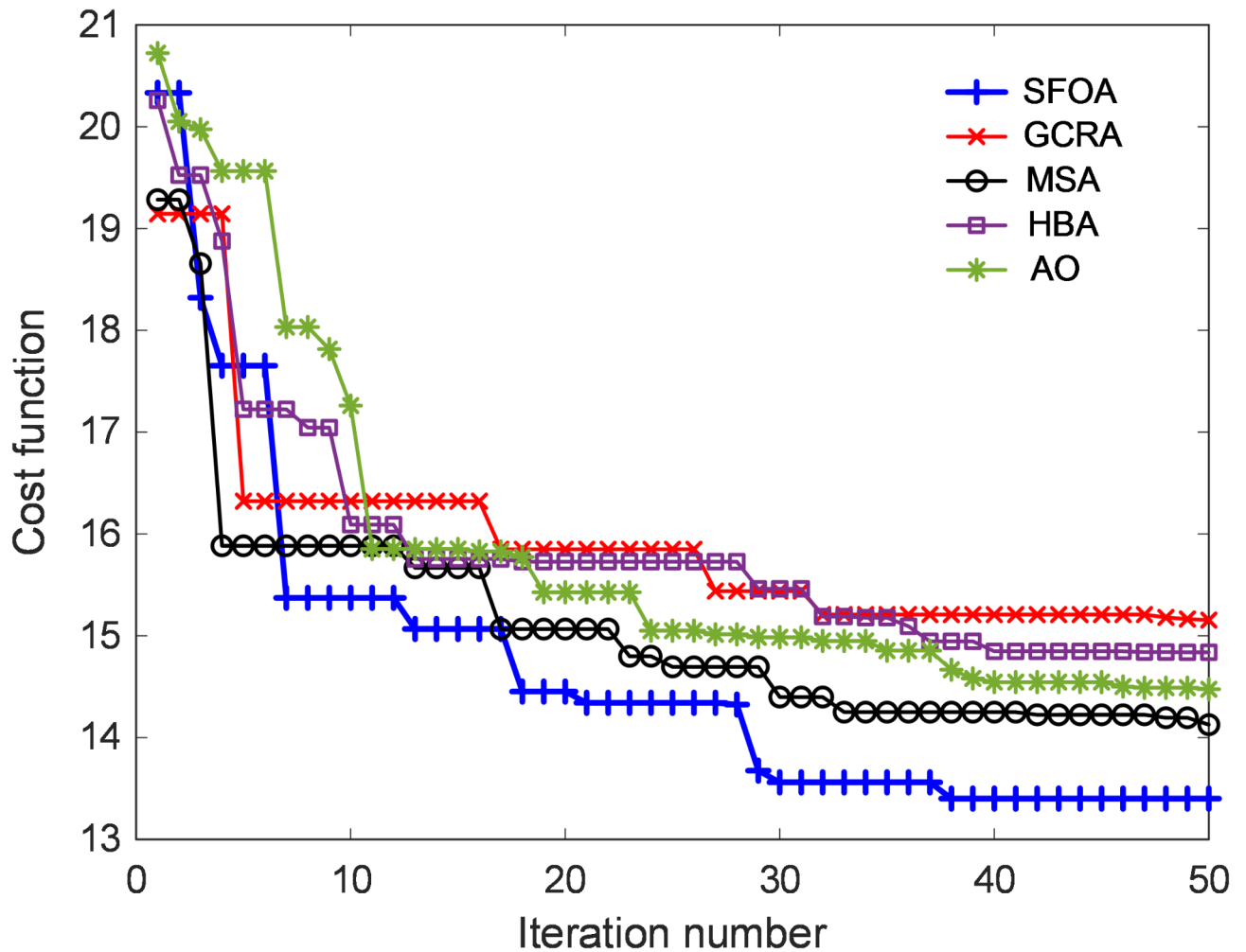


Fig. 8. Change of  $CF$  cost function

time applications, where rapid optimization is essential. Furthermore, SFOA's computational overhead remains manageable, making it a practical choice for embedded and industrial control applications, provided that the hardware meets the necessary processing requirements. The balance between exploration and exploitation ensures that SFOA avoids premature convergence, leading to efficient parameter tuning without excessive computational burden. This result underscores the feasibility of deploying SFOA in real-world industrial systems, where real-time optimization is a critical factor.

According to Table 6, the SFOA algorithm produces superior controller parameter tuning across all metrics when compared to other algorithms. The system achieves enhanced performance through these parameters, which successfully balance stability with responsiveness. Other methods demonstrate inconsistent tuning and suboptimal performance in some regions but the SFOA maintains uniform reliability which leads to enhanced control performance. These results, demonstrate that the SFOA achieves optimal solutions with better efficiency while delivering superior parameters for the 2DOF-PIDA controller compared to other algorithms. The SFOA demonstrates itself to be a powerful and efficient instrument for designing advanced control systems in industrial settings.

#### Time response analysis

A time response analysis was performed on the SFOA-tuned 2DOF-PIDA controller to measure its performance against other metaheuristic algorithms such as GCRA, MSA, HBA, and AO. Figure 9 shows the comparative time responses. Figure 10 provides a detailed view, which allows for better observation of transient behavior.

The data in Table 7 shows that the SFOA has superior performance in time response metrics when compared to other algorithms. The SFOA reacts to changes faster than most competitors because its rise time is less. Its performance features a substantially diminished settling time, which proves it stabilizes systems faster than alternative methods. The minimal overshoot of SFOA shows its capacity to keep control without significant oscillations which helps maintain system integrity and prevent damages. The steady-state error of SFOA remains remarkably low, which enables precise and accurate control to achieve the intended output. Comparisons of time response metrics demonstrate that SFOA provides superior performance in terms of speed and stability along with greater accuracy when contrasted with other modern metaheuristic algorithms. The algorithm

Parameter	SFOA	GCRA	MSA	HBA	AO
$K_p$	8.4566	6.7742	7.4883	15.3677	10.7573
$T_i$	125.4357	148.2619	179.0271	124.7468	91.0258
$T_d$	40.1104	36.4294	34.2824	36.0748	33.3091
$\alpha_d$	0.1533	0.1812	0.1340	0.1887	0.2112
$\beta$	0.9087	1.0661	1.0713	0.7265	0.6370
$\gamma$	7.3544	6.4972	6.0058	4.1054	4.3824
$T_a$	23.6976	23.7971	18.6869	24.4536	20.2475
$\alpha_a$	0.1561	0.2002	0.1838	0.1269	0.1997

**Table 6.** Optimal 2DOF-PIDA controller parameters.

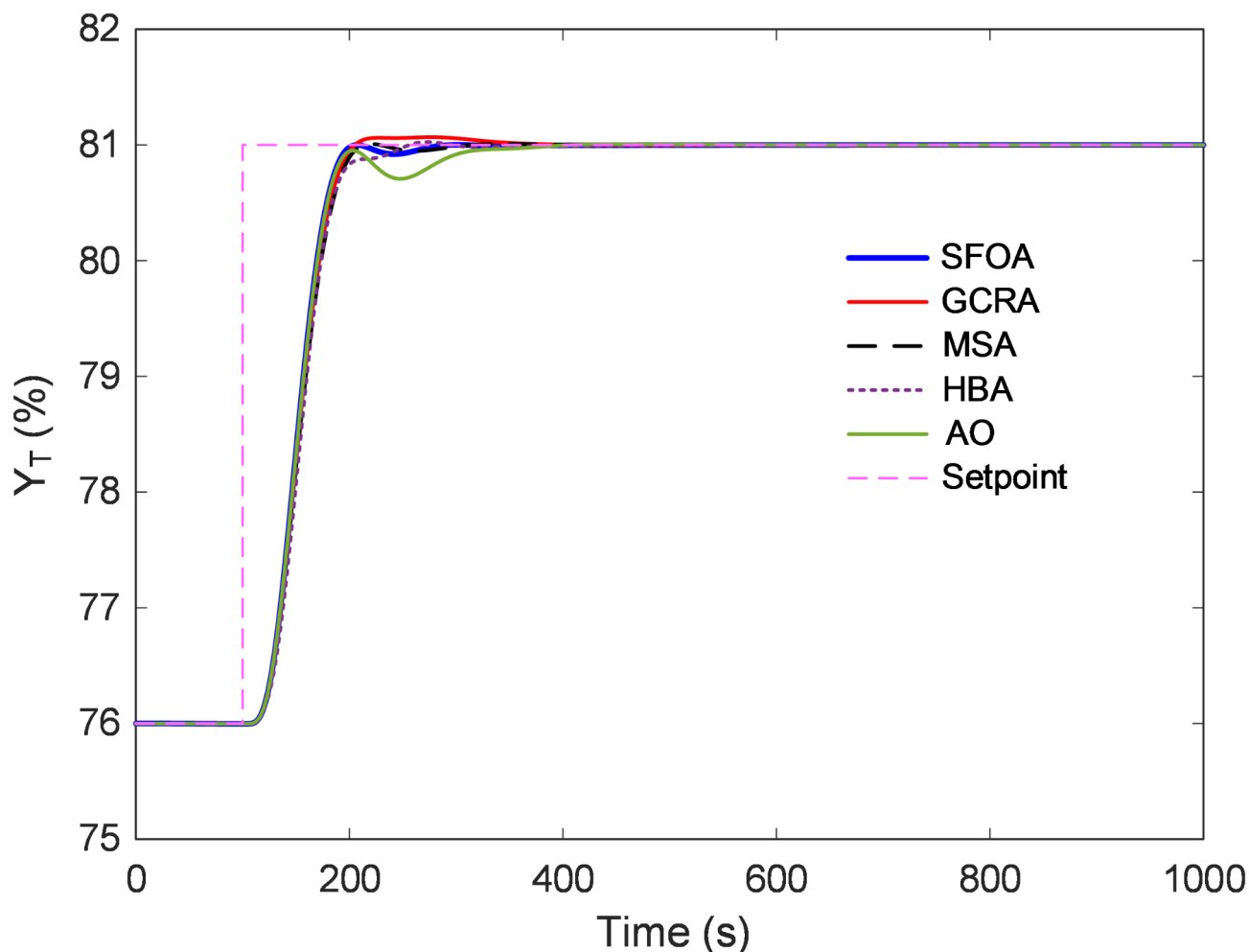


**Fig. 9.** Comparison of time responses.

demonstrates effective and reliable performance within dynamic control systems by reducing both rise time and settling time while minimizing overshoot and steady-state error. The research establishes SFOA as a reliable optimization tool due to its strong performance in controlling systems which makes it essential for sophisticated industrial tasks.

#### Setpoint tracking performance

The performance of the SFOA-tuned 2DOF-PIDA controller in tracking setpoints under different conditions was evaluated to measure its precision and adaptability. The controlled system's time response from Fig. 11 proves that the proposed controller successfully maintains accurate tracking despite dynamic setpoint variations. The SFOA-tuned controller adjusts to setpoint changes quickly with minimal response delay and negligible overshoot in its performance. The controller demonstrates robustness and dependability under dynamic conditions

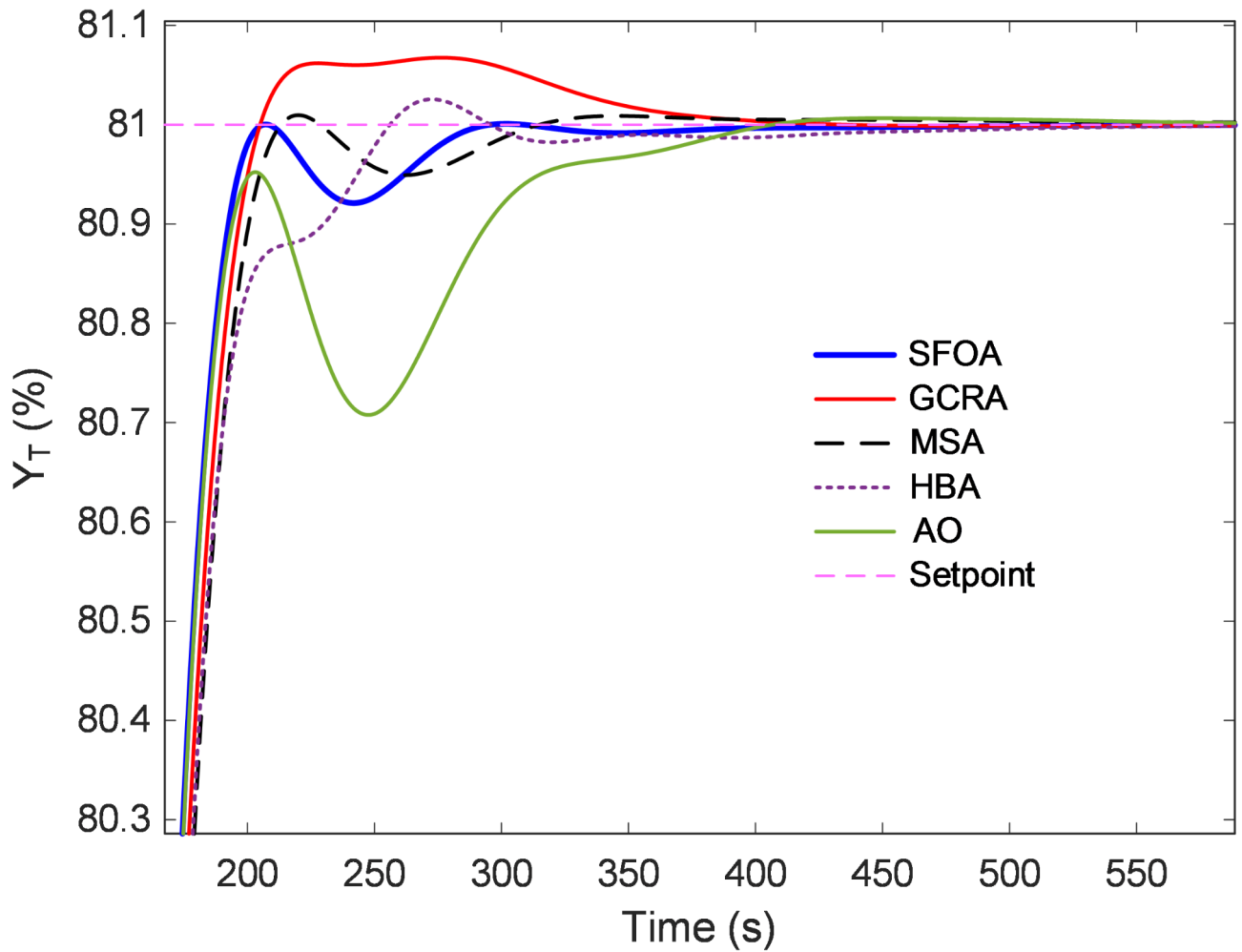


Fig. 10. Zoomed view of Fig. 9.

Time response metric	SFOA	GCRA	MSA	HBA	AO
$t_{rise, norm}$ (s)	50.6027	53.6052	55.8742	53.4604	50.9800
$t_{set, norm}$ (s)	192.5837	196.6382	200.4884	229.9885	294.4251
$O_s, norm$ (%)	0.0183	1.3515	0.1929	0.5132	0.1324
$E_{ss, norm}$ (%)	4.2105E-05	7.8630E-04	0.0048	9.1721E-05	6.4159E-05

Table 7. Comparison of time response metrics for SFOA, GCRA, MSA, HBA and AO.

by successfully stabilizing system outputs to match shifting setpoints. The controller demonstrates efficient management of transient and steady-state conditions through smooth transitions and rapid adjustments, which maintain precise tracking performance throughout various operational ranges. This part shows that the SFOA-tuned 2DOF-PIDA controller achieves superior setpoint tracking results compared to traditional methods by offering faster response times and better stability and precision. Its performance establishes it as an optimal solution for applications that need both dynamic adaptability and consistent precision.

### Disturbance rejection performance

The evaluation of the disturbance rejection capability of the SFOA-tuned 2DOF-PIDA controller focused on how well it maintained system stability and performance when faced with different external disturbances. The applied disturbance signals are illustrated in Fig. 12, which includes variations in key system parameters: Fig. 12 includes illustrations of the applied disturbance signals, which show variations in key system parameters: (a) input signal changes, (b) system load variations, and (c) environmental condition fluctuations.

Figure 13 demonstrates how the SFOA-tuned 2DOF-PIDA controller manages these disturbances with effective suppression of external perturbations. The controller quickly restores system operations to their intended specifications after disturbance events occur. The system’s transient response shows minimal overshoot

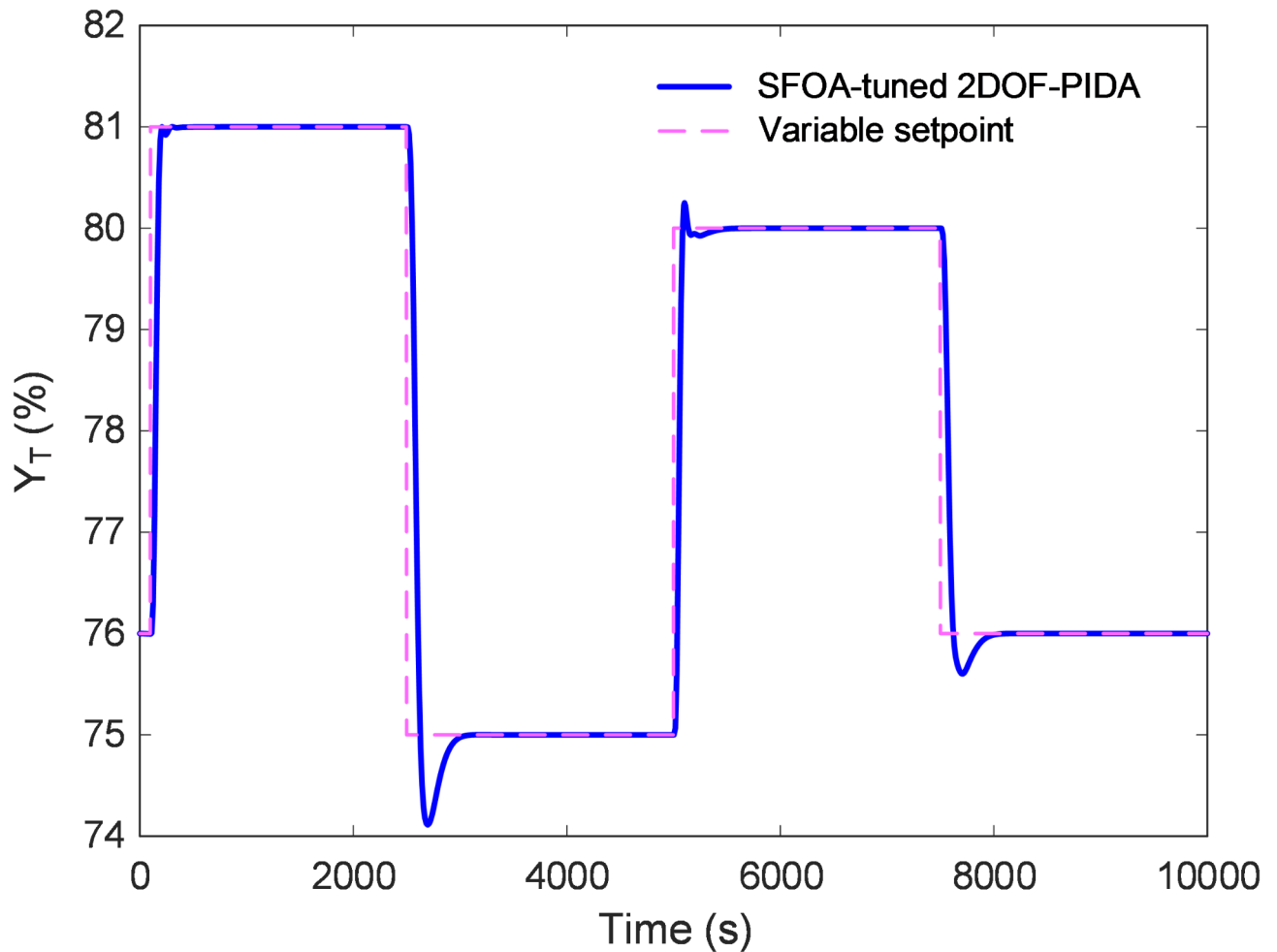


**Fig. 11.** Time response of SFOA-tuned 2DOF-PIDA controlled system under varying setpoint conditions.

and fast settling time, which demonstrates the controller's strength in sustaining system stability during dynamic and difficult scenarios. Test results demonstrate that the SFOA-tuned 2DOF-PIDA controller performs best when rejecting disturbances. The system maintains dependable performance through efficient disruption compensation, making it the preferred choice for control applications that must remain robust against unexpected environmental and operational variations. The controller's ability to reject disturbances makes it extremely suitable for industrial systems that depend on maintaining operational integrity and efficiency through disturbance management.

#### Comparison with SPID, 2DOF-PID and PIDA controllers

Figure 14 illustrates the convergence characteristics of the cost function for different SFOA-tuned controllers, providing a comparative insight into their optimization efficiency. The figure clearly demonstrates that the SFOA-tuned 2DOF-PIDA controller exhibits a faster and more stable convergence trend compared to the SFOA-tuned SPID, SFOA-tuned 2DOF-PID, and SFOA-tuned PIDA controllers. This superior convergence behavior underscores the ability of the 2DOF-PIDA controller, when optimized using SFOA, to rapidly reach an optimal solution with minimal fluctuations. The steep initial descent in the cost function highlights the effective exploitation phase of SFOA, where the algorithm swiftly identifies promising solutions. As iterations progress, the cost function stabilizes, indicating that the controller parameters are effectively fine-tuned, resulting in robust and well-balanced control performance. Notably, the 2DOF-PIDA controller attains the lowest final cost value among the tested controllers, reinforcing its superior adaptability to the nonlinear dynamics of the CSH system.

Table 8 displays the optimal parameters of each controller, which were evaluated alongside their time response characteristics, as shown in Table 9; Fig. 15 visualizes. The tuning data shows the SFOA-tuned 2DOF-PIDA controller reaches an optimal balance between adaptability and stability. The alternative controllers do not have these advanced tuning features which restrict their performance capabilities in dynamic settings.

All controllers tested show slower response times compared to the 2DOF-PIDA controller which demonstrates the quickest rise time and settling time to stabilize the system. The overshoot produced by this controller is significantly lower than those produced by SPID, 2DOF-PID, and PIDA controllers, which results in a more

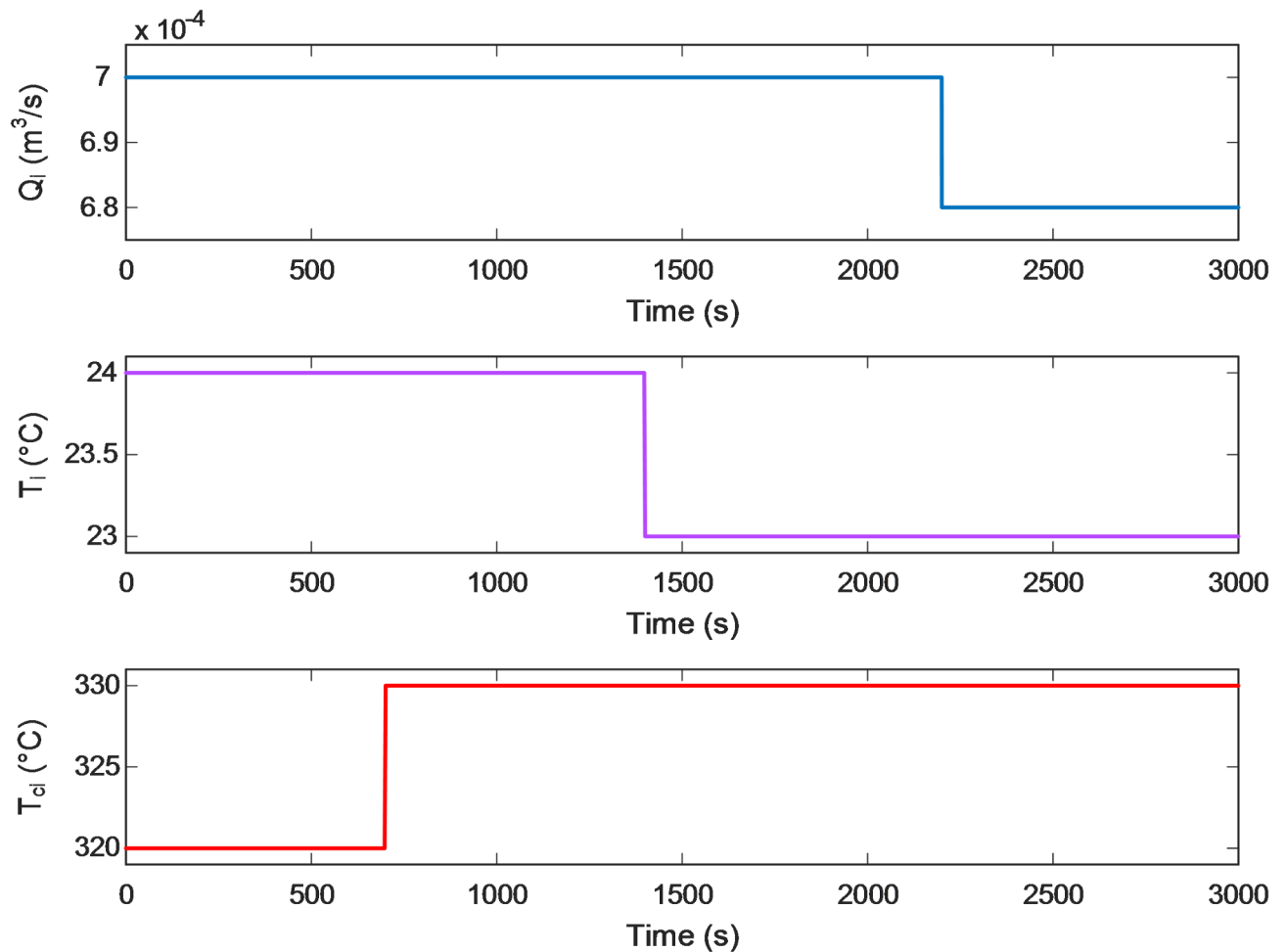


**Fig. 12.** Disturbance signals (a) change of  $Q_i$ , (b) change of  $T_i$ , (c) change of  $T_{ci}$

stable output with minimal variations. The precision and accuracy of the 2DOF-PIDA controller in maintaining the desired system output are demonstrated by its nearly non-existent steady-state error.

The SFOA-tuned 2DOF-PIDA controller performs better than the SPID, 2DOF-PID, and PIDA controllers in every essential performance area, including speed, stability, and accuracy. The 2DOF-PIDA controller's sophisticated structure, combined with its optimal tuning abilities, establish it as the best option for industrial applications needing precise and dependable control performance. The analysis proves that the 2DOF-PIDA controller stands as a strong and functional modern control solution.

### Conclusion and future work

This study proposed a novel metaheuristic-driven control strategy by integrating the 2DOF-PIDA controller with the SFOA for temperature regulation in CSH systems. The results demonstrated the efficacy of this approach in achieving significant improvements in tracking accuracy, disturbance rejection, and robustness compared to recently reports conventional and metaheuristic-based methods. The seamless combination of SFOA's robust optimization capabilities and the enhanced flexibility of 2DOF-PIDA offers a promising solution for controlling highly nonlinear systems. Despite these advancements, several limitations must be acknowledged. First, the proposed approach was validated using simulation environments, which, while highly informative, may not fully capture the complexities of real-world industrial systems. Experimental validation in real-world CSH systems is crucial to confirm its practical applicability. Second, while SFOA has demonstrated excellent performance in tuning controller parameters, its computational efficiency for larger-scale industrial processes with real-time constraints needs further investigation. Moreover, the study primarily focused on CSH systems; thus, generalizing the proposed approach to other types of nonlinear systems requires additional research. From a managerial perspective, the implications of this study are substantial. The integration of advanced control and optimization techniques can lead to significant energy savings, enhanced process efficiency, and reduced operational costs in industries utilizing CSH systems. The robustness of the proposed strategy against disturbances ensures greater reliability in maintaining product quality, which is critical for meeting stringent industry standards and customer expectations. Furthermore, the study provides a foundation for adopting

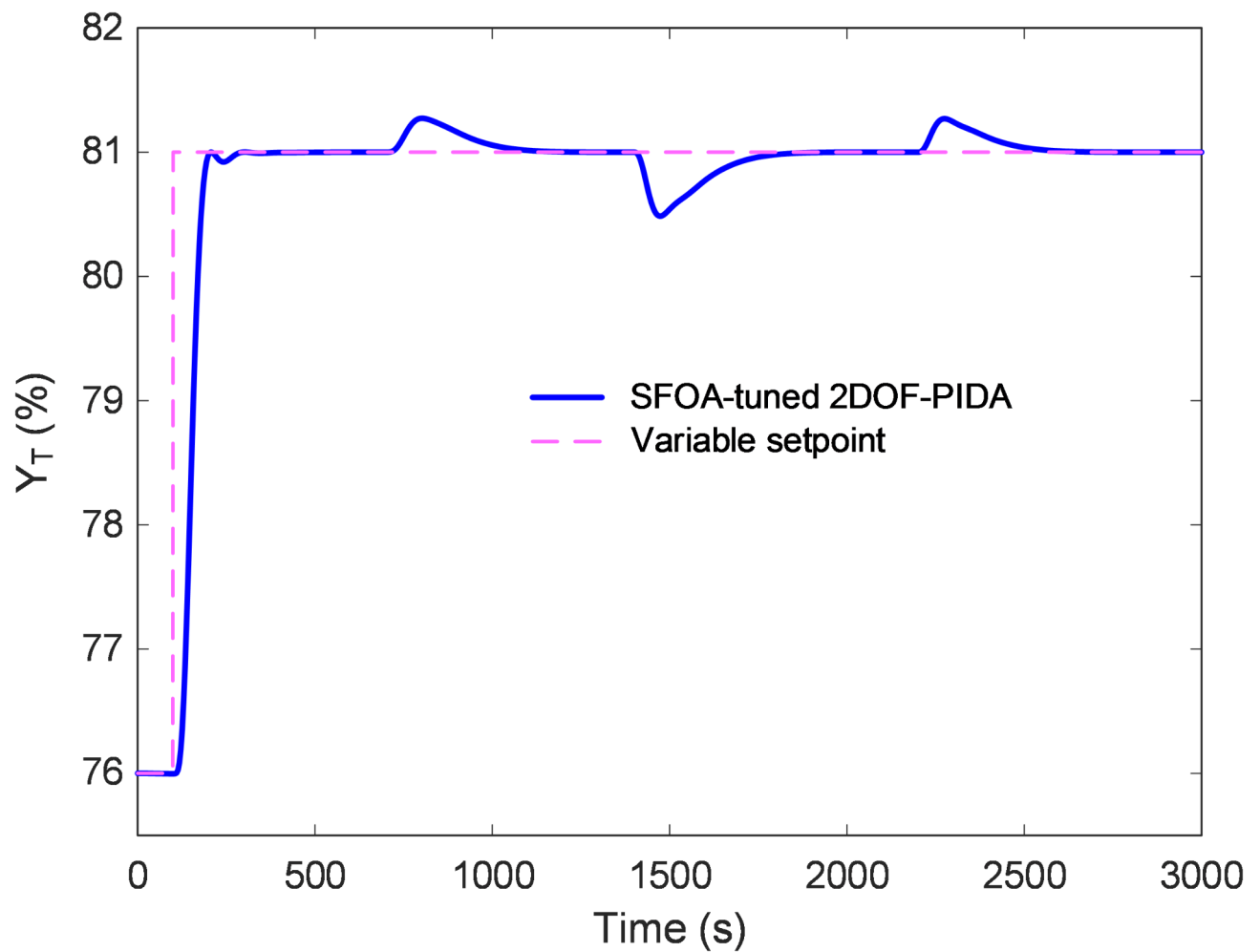


**Fig. 13.** Disturbance rejection ability of SFOA-tuned 2DOF-PIDA controlled system.

similar metaheuristic-driven control strategies in broader industrial contexts, encouraging innovation in process automation and optimization.

Future work should focus on real-world implementation and scalability of the proposed method, exploration of hybrid metaheuristic algorithms to further enhance optimization performance, and addressing computational challenges for real-time applications. Such advancements will pave the way for more sustainable and efficient industrial process control solutions.

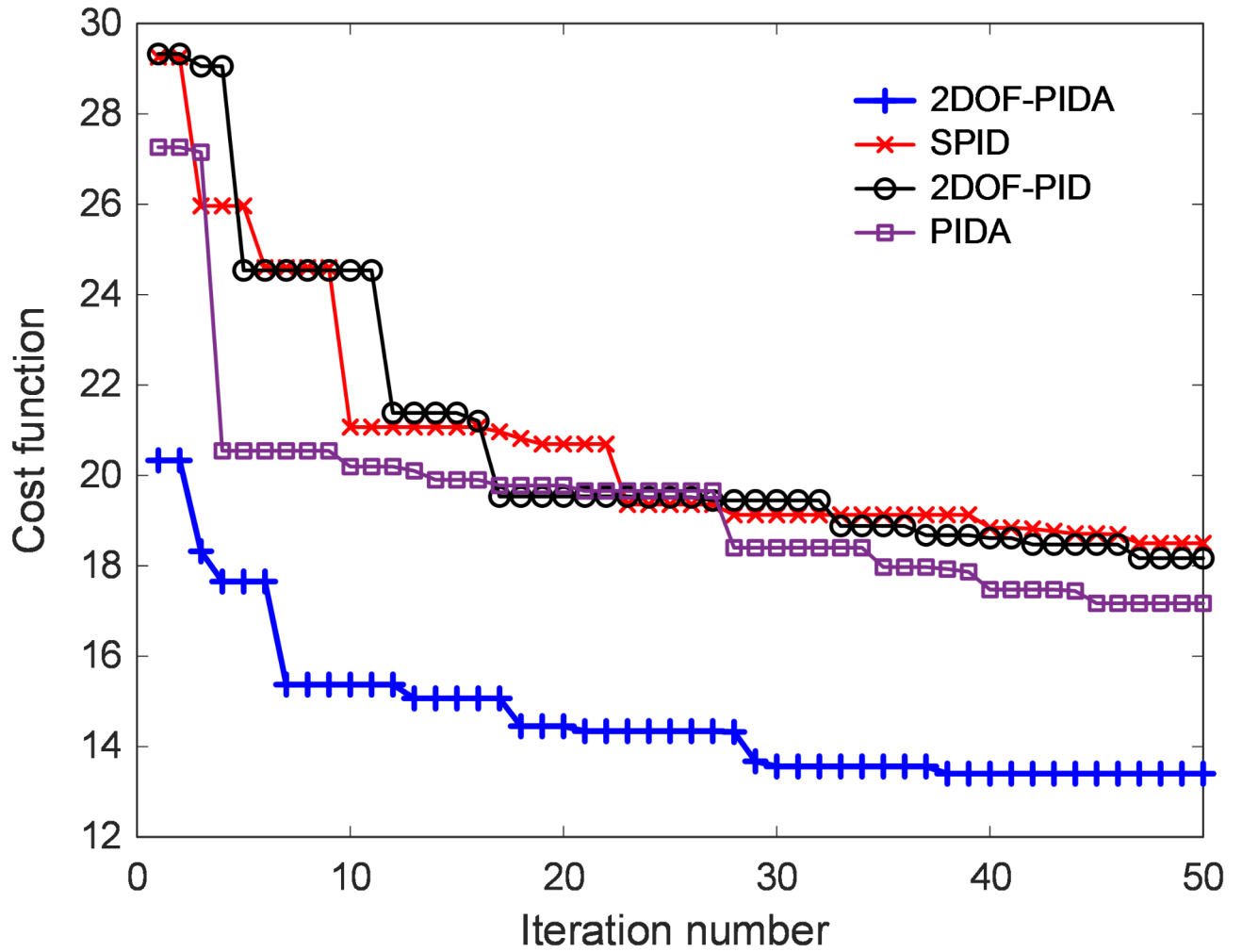


Fig. 14. Change of  $CF$  cost function for SFOA-tuned controllers

Parameter	2DOF-PIDA	SPID	2DOF-PID	PIDA
$K_p$	8.4566	7.2518	9.7872	6.2987
$T_i$	125.4357	149.6405	120.8249	139.3074
$T_d$	40.1104	39.0831	37.4940	41.9279
$\alpha_d$	0.1533	0.0916	0.0815	0.1929
$\beta$	0.9087	-	0.7594	-
$\gamma$	7.3544	-	4.7765	-
$T_a$	23.6976	-	-	8.1738
$\alpha_a$	0.1561	-	-	0.2291

Table 8. Optimal parameters of 2DOF-PIDA, SPID, 2DOF-PID and PIDA controllers tuned by SFOA.

Time response metric	2DOF-PIDA	SPID	2DOF-PID	PIDA
$t_{rise, norm}$ (s)	50.6027	59.9924	57.3929	54.2950
$t_{set, norm}$ (s)	192.5837	293.8057	292.5760	312.4678
$O_s, norm$ (%)	0.0183	1.9945	1.5057	0.7872
$E_{ss, norm}$ (%)	4.2105E-05	0.0224	0.0029	0.0127

Table 9. Comparison of time response metrics for SFOA-tuned controllers.

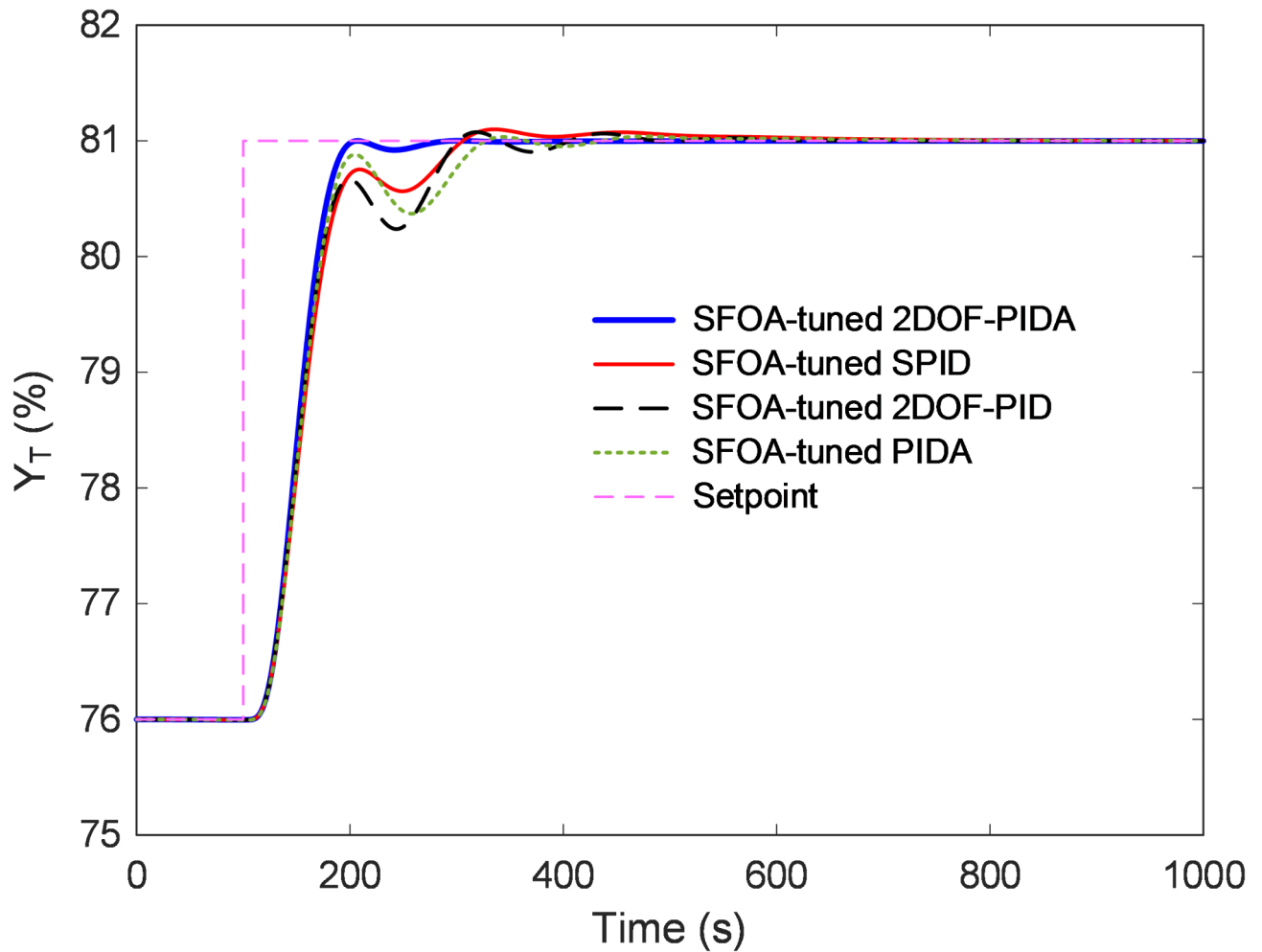


**Fig. 15.** Comparison of time responses for SFOA-tuned controllers.

### Data availability

The datasets used and/or analysed during the current study available from the corresponding author on reasonable request.

Received: 30 January 2025; Accepted: 31 March 2025

Published online: 10 April 2025

### References

1. Song, Y., Zhang, B., Wen, C., Wang, D. & Wei, G. Model predictive control for complicated dynamic systems: a survey. *Int. J. Syst. Sci.* **2025**, 1–26 (2025).
2. Dhanasekar, R. & Vijayachitra, S. Modeling and control of non-linear Csth process using hybrid optimized technique: optimal control of the csth process. *J. Sci. Ind. Res. (JSIR)* **83**(1), 34–45 (2024).
3. Jabari, M., Izci, D., Ekinci, S., Bajaj, M. & Zaitsev, I. Performance analysis of DC-DC Buck converter with innovative multi-stage PIDn (1 + PD) controller using GEO algorithm. *Sci. Rep.* **14**(1), 25612 (2024).
4. Abdel-hamed, A. M., Abdelaziz, A. Y. & El-Shahat, A. Design of a 2DOF-PID control scheme for frequency/power regulation in a two-area power system using dragonfly algorithm with integral-based weighted goal objective. *Energies* **16**(1), 486 (2023).
5. Bhat, V. S., Indiran, T., Selvanathan, S. P. & Bhat, S. Designing multivariable PI controller with multi-response optimization for a pilot plant binary distillation column: a robust design approach. *J. Eng. Des. Technol.* **23**(1), 207–227 (2025).
6. Xiao, Y., Cui, H., Khurma, R. A. & Castillo, P. A. Artificial lemming algorithm: a novel bionic meta-heuristic technique for solving real-world engineering optimization problems. *Artif. Intell. Rev.* **58**(3), 84 (2025).
7. Zhong, C. et al. Starfish optimization algorithm (SFOA): a bio-inspired metaheuristic algorithm for global optimization compared with 100 optimizers. *Neural Comput. Appl.* **2024**, 1–43 (2024).
8. Agushaka, J. O. et al. Greater cane rat algorithm (GCRA): a nature-inspired metaheuristic for optimization problems, *Heliyon* (2024).
9. Hashim, F. A., Houssein, E. H., Hussain, K., Mabrouk, M. S. & Al-Atabany, W. Honey Badger algorithm: new metaheuristic algorithm for solving optimization problems. *Math. Comput. Simul.* **192**, 84–110 (2022).
10. Abualigah, L. et al. Aquila optimizer: a novel meta-heuristic optimization algorithm. *Comput. Ind. Eng.* **157**, 107250 (2021).
11. Ekinci, S., Izci, D., Abualigah, L. & Zitar, R. A. A modified oppositional chaotic local search strategy based Aquila optimizer to design an effective controller for vehicle cruise control system. *J. Bionic Eng.* **20**(4), 1828–1851 (2023).

12. Gao, T., Luo, H., Yin, S. & Kaynak, O. A recursive modified partial least square aided data-driven predictive control with application to continuous stirred tank heater. *J. Process Control* **89**, 108–118 (2020).
13. Mahmood, Q. A. & Nawaf, A. T. Performance analysis of continuous stirred tank heater by using PID-cascade controller. *Mater. Today: Proc.* **42**, 2545–2552 (2021).
14. Tao, M., Gao, T., Li, X. & Li, K. Broad learning aided model predictive control with application to continuous stirred tank heater. *Front. Control Eng.* **2**, 788492 (2021).
15. Wu, X. & Yang, X. A nonlinear subspace predictive control approach based on locally weighted projection regression, *Electronics* **13**(9), 1670 (2024).
16. Ang, G. J. N., Huang, L. & Lim, C. M. Artificial neural network-based controllers for a continuous stirred tank heater process. In *2018 15th International Conference on Control, Automation, Robotics and Vision (ICARCV)* 1414–1419 (IEEE, 2018).
17. Ahmed, J., Amin, S. H. & Fang, L. A multi-objective approach for designing a tire closed-loop supply chain network considering producer responsibility. *Appl. Math. Model.* **115**, 616–644 (2023).
18. Li, X. & Jiang, X. Teaching process control using the CSTH model. In *2018 International Conference on Advanced Control, Automation and Artificial Intelligence (ACAAI 2018)* 163–167 (Atlantis Press, 2018).
19. Rojas, J. D., Arrieta, O. & Vilanova, R. *Industrial PID Controller Tuning* (Springer, 2021).
20. Alfaro, V. M. & Vilanova, R. *Model-Reference Robust Tuning of PID Controllers* (Springer, 2016).
21. Thornhill, N. F., Patwardhan, S. C. & Shah, S. L. A continuous stirred tank heater simulation model with applications. *J. Process Control* **18**, 3–4 (2008).
22. Eibeck, A., Shaocong, Z., Mei Qi, L. & Kraft, M. *Research data supporting: A Simple and Efficient Approach to Unsupervised Instance Matching and its Application to Linked Data of Power Plants* (2024).
23. Mann, G., Hu, B. G. & Gosine, R. Analysis and development of new PID controller tuning rules for first-order processes. *IFAC Proc. Vol.* **30**(25), 169–175 (1997).
24. Åström, K. J. & Hägglund, T. The future of PID control. *Control Eng. Pract.* **9**(11), 1163–1175 (2001).
25. Izci, D., Hekimoğlu, B. & Ekinci, S. A new artificial ecosystem-based optimization integrated with Nelder-Mead method for PID controller design of Buck converter. *Alexandria Eng. J.* **61**(3), 2030–2044 (2022).
26. Abdel-Basset, M., Mohamed, R., Zidan, M., Jameel, M. & Abouhawwash, M. Mantis search algorithm: a novel bio-inspired algorithm for global optimization and engineering design problems. *Comput. Methods Appl. Mech. Eng.* **415**, 116200 (2023).

## Acknowledgements

This research is funded by European Union under the REFRESH—Research Excellence For Region Sustainability and High-Tech Industries Project via the Operational Programme Just Transition under Grant CZ.10.03.01/00/22\_003/0000048; in part by the National Centre for Energy II and ExPEDite Project a Research and Innovation Action to Support the Implementation of the Climate Neutral and Smart Cities Mission Project TN02000025; and in part by ExPEDite through European Union's Horizon Mission Programme under Grant 101139527. The authors would like to express their sincere gratitude to Stanislav Misak for his exceptional supervision, project administration, and overall guidance throughout the course of this project. His expertise and support were instrumental to its success.

## Author contributions

Davut Izci, Serdar Ekinci, Mostafa Jabari: Conceptualization, Methodology, Software, Visualization, Investigation, Writing- Original draft preparation, Mohit Bajaj, Ali Riza Yildiz: Data curation, Validation, Supervision, Resources, Writing - Review & Editing. Seyedali Mirjalili, Lukas Prokop, Vojtech Blazek: Project administration, Supervision, Resources, Writing - Review & Editing.

## Competing interests

The authors declare no competing interests.

## Additional information

**Correspondence** and requests for materials should be addressed to M.B.

**Reprints and permissions information** is available at [www.nature.com/reprints](http://www.nature.com/reprints).

**Publisher's note** Springer Nature remains neutral with regard to jurisdictional claims in published maps and institutional affiliations.

**Open Access** This article is licensed under a Creative Commons Attribution-NonCommercial-NoDerivatives 4.0 International License, which permits any non-commercial use, sharing, distribution and reproduction in any medium or format, as long as you give appropriate credit to the original author(s) and the source, provide a link to the Creative Commons licence, and indicate if you modified the licensed material. You do not have permission under this licence to share adapted material derived from this article or parts of it. The images or other third party material in this article are included in the article's Creative Commons licence, unless indicated otherwise in a credit line to the material. If material is not included in the article's Creative Commons licence and your intended use is not permitted by statutory regulation or exceeds the permitted use, you will need to obtain permission directly from the copyright holder. To view a copy of this licence, visit <http://creativecommons.org/licenses/by-nc-nd/4.0/>.

© The Author(s) 2025